frontiers | Frontiers in Marine Science

TYPE Review
PUBLISHED 15 December 2022
DOI 10.3389/fmars.2022.1031096

OPEN ACCESS

EDITED BY
Dong Feng,
Shanghai Ocean University, China

REVIEWED BY
Yang Lu,
University of Oslo, Norway
Zhifeng Wan,
Sun Yat-sen University, China

*CORRESPONDENCE
Hailong Lu
hlu@pku.edu.cn

SPECIALTY SECTION
This article was submitted to Marine Biogeochemistry, a section of the journal Frontiers in Marine Science

RECEIVED 29 August 2022
ACCEPTED 14 November 2022
PUBLISHED 15 December 2022

CITATION
Liu H, Zhan L and Lu H (2022) Mechanisms for upward migration of methane in marine sediments. *Front. Mar. Sci.* 9:1031096. doi: 10.3389/fmars.2022.1031096

Mechanisms for upward migration of methane in marine sediments

Haotian Liu[1,2], Linsen Zhan[2] and Hailong Lu[2*]

[1]College of Engineering, Peking University, Beijing, China, [2]Beijing International Center for Gas Hydrate, School of Earth and Space Sciences, Peking University, Beijing, China

Methane, a non-negligible component of the global carbon budget, could be discharged upward through marine sediments to ocean floor by certain migration mechanisms. Although quite some studies have been conducted, the mechanisms for methane migration have not been well reviewed yet, especially in hydrate-bearing sediments. In this study, methane migration mechanisms are classified into diffusion and advection processes which include water movement, free gas flow, sediment failures, and recently developed gas migration through hydrate channels. The occurrence of natural gas hydrate might affect methane migration in three ways: (1) reducing the permeability of marine sediments and consequently hindering the upward movement of methane either in gas or liquid phase, (2) enhancing the geomechanical strength of marine sediments, which prevents the creation of new pathways for methane escape by sediment failures, and (3) benefiting upward methane migration by constructing hydrate channels at the interface of continuous gas columns. Generally, dissolved methane could hardly break through the gas hydrate stability zone and sulfate-methane transition zone because of the high consumption rate for methane in these two zones. For free methane gas, the capillary force is a strong resistance to free gas flow in porous sediments. However, whether for dissolved methane or free methane gas, discharge along pre-existing fractures or failure surfaces might be considerable. In addition, methane discharge by gas flow through hydrate channels is still hard to constrain. Finally, based on current research uncertainties in constraining the methane flux to the ocean, the research outlook is also addressed. It is suggested that more investigations should be conducted in three aspects: the flow characteristic of high-permeability conduits, the quantitative correlations of geomechanical properties and hydrate distribution, and the occurrence conditions of hydrate channels.

KEYWORDS

diffusion, water movement, free gas flow, sediment failure, hydrate channel, gas hydrate

1 Introduction

Methane is a potent greenhouse gas with a warming potential that is ~23 times stronger than carbon dioxide (Stocker, 2014), and can be generated in marine sediments primarily by biodegradation of organic matters or thermal decomposition of organic matters in depth (Reeburgh, 2007; Timmis et al., 2010; You et al., 2019). The methane would migrate upward through marine sediments, potentially escaping into ocean or even to atmosphere (Liu et al., 2019). Considering the vast area of seafloor, the methane flux across seafloor to the ocean is expected to account for a non-negligible part of the global carbon budget (Dickens, 2003; Weber et al., 2019). For example, Ruppel and Kessler (2017) estimated the global methane flux in the range of 16 to 3200 Tg yr^{-1} based on an assumption that the dissolved methane concentration and the aerobic oxidation rate for methane are both steady. However, it is quite difficult to constrain the methane flux accurately, considering the spatial heterogeneity of marine sediments and the difference in mechanisms for methane transport. That is, different mechanisms for methane transport might dominate in different geological settings, contributing unevenly to the methane flux. The limited data available might also lead to the estimation of the methane flux with a variance of orders of magnitude over different regions or even at different spots in the same region (Linke et al., 1994; Tryon et al., 1999). Moreover, some processes might be involved with methane, e.g., hydrate formation/degradation (Ruppel and Waite, 2020), methane dissolution/exsolution (Sultan et al., 2020), and oxidation of methane (Barnes and Goldberg, 1976), and they could also exert a certain influence on upward methane migration, complicating the estimation of the methane flux. Therefore, it is too arbitrary to obtain the global methane flux by simply extrapolating from the locally-representative data in field surveys. To understand methane migration in marine sediments, clarification on the methane migration mechanisms is required for constraining the methane flux from sediments to the ocean.

In this review, the mechanisms for upward methane migration in gas hydrate systems are summarized, including diffusion and advection, such as water movement, free gas flow, sediment failures, and recently developed gas flow through hydrate channels, with the effects of hydrate formation and anaerobic oxidation on methane. The contribution of each mechanism to the methane flux to the ocean is also qualitatively evaluated. The future research outlook is also addressed based on current research uncertainties in constraining the methane flux to the ocean. This review aims to (1) provide a comprehensive understanding of different methane migration mechanisms associated with gas hydrate systems that can cause methane seepage and (2) point out future research topics that should be strengthened to help constrain the methane flux to the ocean.

2 Migration mechanisms

2.1 Upward methane diffusion

Diffusion, one of the most fundamental mechanisms for mass transfer, is the movement of small particles (e.g., atoms, ions, molecules) from a region with higher concentration to that with lower concentration, driven by a gradient in Gibbs free energy or chemical potential. When one solute distributes unevenly in bulk water, its steady diffusive flux could be obtained from Fick's First Law at the macroscale (Fick, 1855; Atkins and de Paula, 2021),

$$J = -D \nabla c_{aqu}^{CH_4} \quad (1)$$

where J is the diffusive flux ($nL^{-2}T^{-1}$); D is the diffusion coefficient (L^2T^{-1}); $c_{aqu}^{CH_4}$ is the dissolved methane concentration (nL^{-3}). In water saturated porous media, the matters dissolved into pore water could also be transferred by diffusion through throats between grains. Previous studies have indicated that the diffusive flux in porous media J_e could be described approximately by $J_e = -D_e \nabla c_{aqu}^{CH_4}$ similar to Fick's First Law (Perkins and Johnston, 1963). The law is a good tool for calculating the diffusive methane flux according to the measured methane concentration profile. For example, Cao et al. (2021) obtained the diffusive methane flux of five sites in pockmark areas offshore Fujian province ranging from 2.89 – 15.17 × 10^{-2} mmol/(m^2yr) by Fick's First Law.

2.1.1 Effective diffusion coefficient

The effective diffusion coefficient D_e in porous media is generally lower than the coefficient D in bulk water, since diffusion in porous media would be weakened by the tortuosity of the flow paths (Ullman and Aller, 1982). This means D_e is dependent on porosity and pore structures (Ullman and Aller, 1982; Iversen and Jørgensen, 1993), besides pressure, temperature, and concentration as in bulk water. According to Iversen and Jørgensen (1993), the effective diffusion coefficient for methane in marine sediments at 4 °C (near the seafloor temperature) lies between 10^{-8} and 10^{-9} m^2s^{-1}, which indicates that methane diffusion might be an extremely inefficient way for methane migration in marine sediments.

2.1.2 Concentration gradient of methane

As a consequence of the heterogeneity of methane sources, pressure, temperature, salinity, and lithology (Handa, 1990; Ginsburg and Soloviev, 1997; Brereton et al., 1998; Nole et al., 2016), methane concentration is normally uneven in marine sediments. In the vertical direction, the effects of pressure and temperature are preferentially considered, since the geothermal gradient and the hydrostatic gradient are common in marine sediments.

Methane solubility is the maximum concentration of dissolved methane at a given *P-T* condition, here regarded as the reference value of the methane concentration. Methane solubility could be classified into methane gas solubility and methane hydrate solubility (You et al., 2019). The former refers to the dissolved methane concentration when dissolved methane and free methane gas are at thermodynamic equilibrium. Duan and Weare (1992) suggested that higher methane gas solubility can be obtained at lower temperature and higher pressure. On the other hand, methane hydrate solubility represents the dissolved methane concentration when dissolved methane and methane hydrate are at thermodynamic equilibrium. Methane hydrate solubility increases with temperature and decreases with pressure (Henry et al., 1999).

The vertical temperature and pressure distributions have opposite effects on these two methane solubilities, considering that temperature and pressure both increase with depth. According to previous calculations (Xu and Ruppel, 1999; You et al., 2019), these two solubilities are both sensitive to temperature change in geological systems. That says, methane hydrate solubility increases with depth, while methane gas solubility slightly decreases with depth, as shown in Figure 1.

2.1.3 Contribution of diffusion

Although the upward-decreasing methane hydrate solubility provides a driving force for vertical methane diffusion, the diffusion plays a minor role in transporting methane to the ocean, especially over long distances (Max, 2003; You and Flemings, 2021). According to some field surveys conducted in ocean or lake (Keller and Stallard, 1994; Sauter et al., 2006; Delsontro et al., 2010), methane diffusion only takes a minor

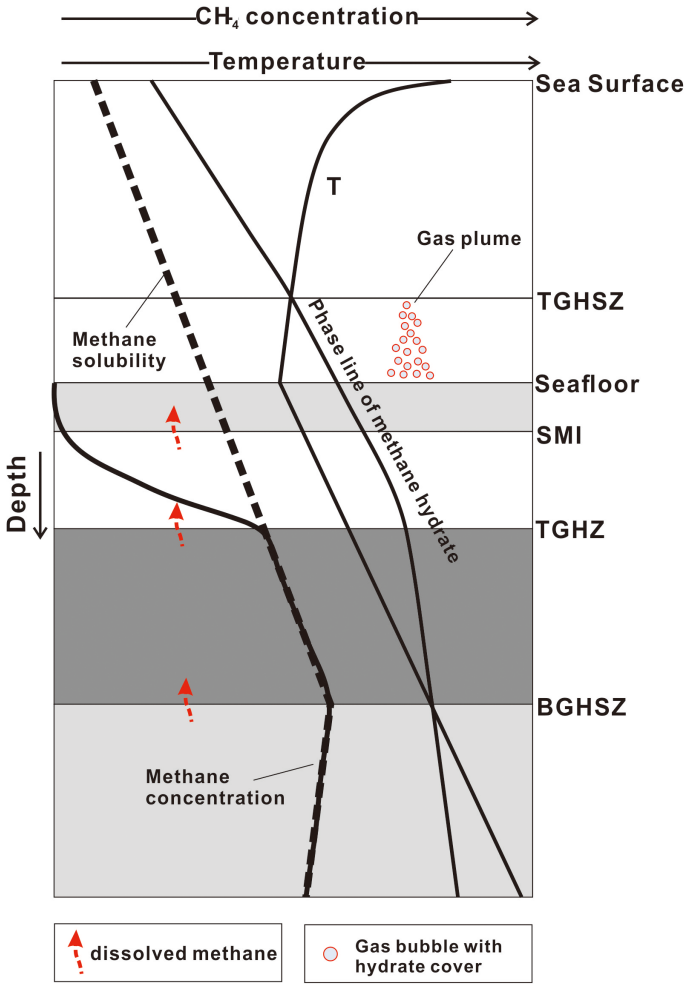

FIGURE 1
Conceptual profile of dissolved methane concentration and solubility [modified from Xu and Ruppel (1999)]. The two solubility curves intersect at the base of gas hydrate stability zone (BGHSZ). TGHSZ, top of gas hydrate stability zone; SMI, sulfate-methane interface; TGHZ, top of gas hydrate zone. Thicknesses of each layer are not to scale.

part of overall methane discharge across seafloor or lake bottom, as the result of the low diffusion coefficient and the low concentration gradient combined. As suggested by Algar et al. (2011a), a timescale of weeks to months would be taken for dissolved methane to pass through tens of centimeters thick sediments based on the Einstein-Smoluchowski equation (Islam, 2004), allowing for the conversion of most dissolved methane into methane hydrate in the gas hydrate stability zone (GHSZ). The upward-decreasing methane hydrate solubility means hydrate formation is even easier in shallower sediments, since the amount of hydrate formation is dependent on the excessive dissolved methane concentration over methane solubility (Ginsburg and Soloviev, 1997), which indicates that GHSZ is a strong barrier for methane diffusion (Xu and Ruppel, 1999). In addition, the methane escaping from GHSZ would be oxidized with sulfate by a process known as sulfate-driven anaerobic oxidation of methane (SD-AOM): CH_4(aq) + SO_4^{2-} (aq) → HCO_3^- (aq) + HS^-(aq) + H_2O, in which the diffusive methane is usually completely consumed (Barnes and Goldberg, 1976; Reeburgh, 2007; Dale et al., 2009; James et al., 2016; Egger et al., 2018; Mau et al., 2020; De La Fuente et al., 2022). For example, Dale et al. (2008) pointed out that less than 1% of the upward dissolved methane flux could reach the ocean under the restriction of SD-AOM. The SD-AOM communities could even improve their metabolic activities to balance the increase of the methane flux (Nauhaus et al., 2002). The sediment column in which SD-AOM occurs is therefore termed as sulfate-methane transition zone (SMTZ). This means SMTZ is another efficient barrier for methane migration besides GHSZ. Despite the low efficiency of diffusion for methane discharge, diffusion is a universal process for methane migration in marine sediments. A mud layer could be an effective seal for gas bubble motion, but cannot arrest the diffusion of dissolved methane according to previous experiments (Miller, 1980).

2.2 Upward methane advection

Advection is another mechanism for mass transfer by the bulk motion of fluid. In porous media, fluid flow could be affected by porosity and pore structures, besides fluid viscosity and pressure distribution as in free flow. In marine sediments, the vertical advection of the dissolved or free methane might cause methane discharge to the ocean. By pathways and methane phase states, the upward methane advection could be classified into water movement, free gas flow, sediment failures, and gas flow through hydrate channels.

2.2.1 Water movement

The upward water movement in marine sediments could be driven by overpressure gradient, buoyancy, and osmotic pressure. Regardless of driving force, the methane flux could be obtained by the following equation,

$$q_{CH_4} = c_{aqu}^{CH_4} q_{aqu} \tag{2}$$

where $q_{CH4}$is the upward methane flux ($nL^{-2}T^{-1}$); q_{aqu} is the water flux (LT^{-1}), as determined by driving force.

2.2.1.1 Driving force

2.2.1.1.1 Overpressure gradient

In active marine margins, external forces with high sedimentation rates and compaction would induce vertical fluid flow with velocities of several millimeters to 1-2 meters per year (James et al., 2016). The vertical water flux could be calculated according to Darcy's Law (Darcy, 1856; Bear, 1988) as follows,

$$q_{aqu} = -\frac{k}{\mu_w}\left(\frac{\partial P_w}{\partial z} + \rho_w g\right) \tag{3}$$

where q_{aqu} is the water flux (LT^{-1}); k is the permeability (L^2); μ_w is the dynamic water viscosity ($ML^{-1}T^{-1}$); P_w is the water pressure ($ML^{-1}T^{-2}$); P_w is the water density (ML^{-3}); g is the gravitational acceleration (LT^{-2}). The equation shows that the upward water flux is the function of the permeability and overpressure gradient $\partial P_w/\partial z+\rho_w g$ (i.e., the hydrostatic pressure gradient subtracted from the fluid pressure gradient). For example, Dugan and Flemings (2000) suggested that fluid is expelled laterally and vertically upward with an average Darcy velocity of 0.5 mm/yr in New Jersey continental slope through numerical simulation based on Darcy's Law.

The overpressure gradient could be caused by the external loading decrease and the internal pressure increase. The external loading decrease might occur in short-time processes, such as daily tidal variations (Hsu et al., 2013; Sultan et al., 2020) or in geologic-timescale activities like iceberg retreating (Dessandier et al., 2021). Another cause for the genesis of the overpressure gradient is the increase of pore pressure in sediments, which could be generated by physical processes [e.g., disequilibrium compaction in rapid sedimentation (Osborne and Swarbrick, 1997; Dugan and Flemings, 2000; Dugan and Sheahan, 2012), light fluid migration from depth (Osborne and Swarbrick, 1997), fluid aquathermal expansion (Bethke, 1986; Mello et al., 1994), and tectonic movements (Li et al., 2022)], or chemical processes [e.g., diagenesis and hydrocarbon generation (Bethke, 1986; Ma et al., 2021)]. For hydrate-bearing sediments, hydrate dissociation caused by the change of ambient conditions could also pressurize surrounding water, since gas released from hydrate dissociation would expand in pores (Xu and Germanovich, 2006). Additionally, hydrate-bearing sediments could act as good seals for gas migration (Hornbach et al., 2004; Ma et al., 2021). For example, Flemings et al. (2003) suggested that fluid pressure beneath hydrate layers even reaches ~70% of the lithostatic stress in Blake Ridge.

Except for those naturally-occurring overpressure, human activities could also induce localized overpressure. For instance, overpressure in marine sediments might be induced during drilling operations or hydrocarbon production processes, since external fluids are generally injected into marine sediments to ensure smooth drilling or enhance recovery (Dugan and Sheahan, 2012). Therefore, gas hydrate must be carefully developed to avoid man-made large-scale methane leak (Zhang and Zhai, 2015), although it has been viewed as a promising energy source (Boswell and Collett, 2011).

2.2.1.1.2 Buoyancy

When less dense water is surrounded by high-density water, it could rise spontaneously by buoyancy. The water flux could be calculated as follows,

$$q_{aqu} = -\frac{k}{\mu_w}(\Delta\rho g) \tag{4}$$

where $\Delta\rho$ is the density difference between the two fluids (ML^{-3}). For homogeneous sediments, Cardoso and Cartwright (2016) estimated the velocity of upward fluid flow at 0.15m/yr and 0.75m/yr for thermal and solute sources, respectively.

In marine sediments, the buoyancy of water phase can be induced by thermal or solute sources. The former represents the decrease of water density due to heating, while the latter means the density change caused by the diffusion of solutes. These two sources could also occur in gas hydrate formation or dissociation processes. For instance, heat would be released during hydrate formation or less dense fresh water would be released during hydrate dissociation (Cardoso and Cartwright, 2016).

2.2.1.1.3 Osmotic effects

The osmotic effects would cause a flow of water from the dilute solution to the strong solution through semipermeable membranes. Cardoso and Cartwright (2016) proposed that marine sediments could be regarded as a special case of semipermeable media for methane movement, considering the strong absorption of marine sediments for methane molecules. By osmotic pressure, methane-free seawater would move downward through marine sediments to displace methane-saturated pore water upward along high-permeability conduits. Based on field measurements, Cardoso and Cartwright (2016) gave an estimation of the water flux by considering a balance of osmotic and viscous forces as follows,

$$q_{aqu} \sim \frac{2k_f}{a\mu_w}P_o = \frac{2k_f}{a\mu_w}\sigma_0 c_0 RT \tag{5}$$

where k_f is the permeability of high-permeability conduits (L^2); P_o is the osmotic pressure ($ML^{-1}T^{-2}$); σ_0 is the reflection coefficient (1); c_0 is methane solubility (nL^{-3}); R is the universal gas constant ($ML^2T^{-2}n^{-1}K^{-1}$); T is the temperature (K); a is the radius of high-permeability conduits (L).

2.2.1.2 Permeability

The permeability of marine sediments regulates the amount of water that could pass through the overlying sediments to the ocean, reflecting the resistance of sediment grains to free flow. Reagan et al. (2011) suggested that the permeability of marine sediments is a predominant factor controlling methane discharge to the ocean by numerical simulation. The permeability of marine sediments is dependent on porosity, pore structures, compaction degree, cementing types, clay content, with extra hydrate saturation S_h and hydrate morphology for hydrate-bearing sediments (Lijith et al., 2019). According to field surveys, the permeability of marine sediments exhibits a great variance of orders of magnitude, ranging from 10^{-8} m^2 for sands to 10^{-19} m^2 for consolidated muds (Max, 2003; Spinelli et al., 2004). The permeability in hydrate-occurring continental margins also shows variance. For instance, the permeability in production interval is just a few mDs (1 mD=10^{-15} m^2) in China's first production test (Ye et al., 2020), while it is around 10^2 mDs at the Nankai Trough (Konno et al., 2010).

For hydrate-bearing sediments, gas hydrate precipitating in pores increases the resistance to gas/water flow. At the macroscale, the extra resistance is reflected by the reduction of sediment permeability, even by orders of magnitude, as suggested by previous experiments (Kang et al., 2016). Free gas accumulations beneath hydrate-bearing sediments, a typical feature of gas hydrate reservoirs, are widely observed with bottom simulating reflectors (BSRs) indicating hydrate reservoirs (Haacke et al., 2007; Hornbach et al., 2012; Li et al., 2018), which exhibits the seal capacity of hydrate-bearing sediments. The pore habits, spatial distribution, and hydrate saturation are expected to be critical factors for the permeability of hydrate-bearing sediments (Ren et al., 2020). Some widely-used permeability models are classified into theoretical analyses, empirical models, and numerical simulation models, as shown in Table 1. In addition to these prediction models, the actual permeability of hydrate-bearing sediments was also extensively measured by direct flow tests (Kumar et al., 2010; Li et al., 2017; Dai et al., 2019; Shen et al., 2020), numerical simulation combined with computed tomography (CT) images (Zhang et al., 2020; Pan et al., 2021; Sun et al., 2021), and *in situ* measurements with downhole tools (Fujii et al., 2015). Those permeability models in Table 1 are often used as the benchmarks of actual permeability tests. Both the models and the actual measurements indicate that the permeability decreases with hydrate saturation, although the decrease rate varies in different models and measurements.

2.2.1.3 Methane concentration

As mentioned above, methane solubility in pore water could be classified into methane gas solubility and methane hydrate solubility. No matter which type of methane

TABLE 1 Prediction models for water permeability in the presence of gas hydrate.

Type	Model	Formula	Fitting parameter	Reference	Remark
Theoretical analyses	Tokyo	$k(S_h)=k_0(1-S_h)^2$		(Masuda et al., 1997)	Original Tokyo's model
	PCTM	$k(S_h) = k_0[1 - S_h^2 + 2(1 - S_h)^2/lnS_h]$		(Kleinberg et al., 2003)	PF
		$k(S_h)=k_0(1-S_h)^2$		(Kleinberg et al., 2003)	GC
	SCPM	$k(S_h)=k_0(1-S_h)^4$		(Dai and Seol, 2014)	PF
		$k(S_h)=k_0(1-S_h)^2$		(Dai and Seol, 2014)	GC
Empirical model	Tokyo	$k(S_h)=k_0(1-S_h)^N$	N	(Masuda et al., 1997)	
	SDR	$k(S_h) = C\phi^4 T_{2LM}^2$		(Kleinberg et al., 2003)	T_{2LM} is the logarithmic mean value of the T2 distribution
	KGM	$k(S_h) = k_0(1 - S_h)^{n+2}/(1 + S_h^{0.5})^2$	n (Archie saturation exponent)	(Kleinberg et al., 2003)	PF
		$k(S_h)=k_0(1-S_h)^{n+1}$		(Kleinberg et al., 2003)	GC
	LBNL	$k(S_h)=k_0[(\phi(S_h)-\phi_c)/(\phi_0-\phi_c)]^n$	n typically ranging from 2 to 3	(Moridis, 2014)	
Numerical simulation	Modified KGM	$k(S_h)=k_0[(1-S_h)^3/(1+2S_h)^2]$		(Dai and Seol, 2014)	PNM
	Linear regressions	$k(S_h) = k_0[\frac{(1 - S_h)^3}{(1 + 2.094S_h - 6.691S_h^2 + 6.837S_h^3)^2}]$		(Kang et al., 2016)	PF; LBM
		$k(S_h) = k_0[\frac{(1 - S_h)^3}{(1 - 0.543S_h - 0.148S_h^2 + 1.886S_h^3)^2}]$		(Kang et al., 2016)	GC; LBM
		$k(S_h) = \tau_{cr}^{-6} r_{cr}(1 - S_h)^3$		(Hou et al., 2018)	LBM; τ_{cr} is the relative control seepage channel tortuosity; r_{cr} is the relative control flow channel size

PCTM, parallel capillary tube model.
SCPM, simple cubic packing model.
SDR, Schlumberger-Doll Research model.
KGM, Kozeny grain model.
LBNL, Lawrence Berkeley National Laboratory model.
PF, pore-filling.
GC, grain-coating.
PNM, pore network model.
LBM, Lattice Boltzmann method.

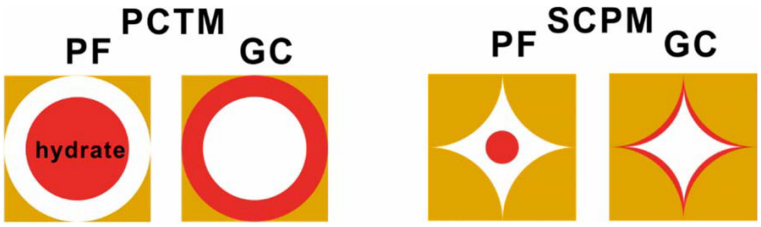

solubility is, it could be predicted accurately according to existing equations of state (Duan and Weare, 1992; Henry et al., 1999). Davie et al. (2004) suggested that methane solubility ranges roughly from 0.05 to 0.2 M (mole per liter) at depths from 0 to 600 meters below seafloor (mbsf) in selected sites.

2.2.1.4 Contribution of water movement

Methane discharge alongside the upward water movement is expected to be of minor importance, since methane solubility is small and the driving force would supposedly dissipate over long migration distance (Max, 2003). Considering that the methane flux is low, GHSZ and SMTZ are still powerful barriers to

methane migration (James et al., 2016; You et al., 2019; Ruppel and Waite, 2020), as in the upward methane diffusion. The limited literatures also indicate that the real-time fluid flux across seafloor is low and transient (Tryon et al., 1999; Torres et al., 2002; Sauter et al., 2006).

However, high water flux might occur if fractures, faults, scarps, or other high-permeability pathways exist, accompanied by striking phenomena including cold seeps, mud volcanos, and pockmarks on the seabed (Ma et al., 2021). Linke et al. (1994) measured a fluid velocity as high as 10^5 cm/yr in seep sites, and calculated a methane flux of 120 mmol/(m^2day) on Hydrate Ridge. Stranne et al. (2019) suggested that fracture flow with high velocities could weaken the SD-AOM efficiency by numerical simulation. In addition, polygonal faults developed in fine-grained sediments weaken the seal capacity of marine sediments, providing new pathways for upward water migration (Ma et al., 2021). Berndt (2005) suggested that pipe structures extending from deep polygonal faults are probably the evidence of fluid migration along fault planes.

Human activities are also worrying since these activities might induce more violent increase of fluid pressure than natural processes. It should be noted that when water pressure is high enough to overcome the lithostatic stress, sediments failures (e.g., hydraulic fracturing and fault slips) would occur, facilitating the upward movement of methane (Hornbach et al., 2004; Dugan and Sheahan, 2012).

2.2.2 Free gas flow

Methane bubbles would nucleate if the methane concentration exceeds its solubility. For hydrate-bearing sediments, hydrate can also dissociate into free methane gas and water when *P-T* condition resides out of the gas hydrate stability zone. These methane bubbles would migrate upward by buoyancy, with the possibility of reaching the ocean singly or as a plume. For example, more than 250 gas plumes were observed emitting from the seafloor of the West Spitsbergen margin above the upper limit of GHSZ (Graham, 2009). The free gas flow in porous sediments is composed of three processes: buoyant movement, capillary trapping, and pressure-driven flow.

2.2.2.1 Buoyant movement

When gas bubbles are small enough or flow space is large enough (e.g., fractures), these bubbles could move freely without being deformed by grains in the vertical direction, as methane gas is still buoyant relative to pore water even at large depth (Max, 2003). The upward velocity of gas bubbles v_b (LT^{-1}) could be estimated by the Stoke's law (Zheng and Yapa, 2000),

$$v_b = \frac{g(\rho_w - \rho_g)d^2}{18\mu_w} \tag{6}$$

where ρ_w is the water density (ML^{-3}); p_g is the density of gas bubbles (ML^{-3}); d is the diameter of gas bubbles (L). By the equation, the upward velocity of a bubble with a diameter of 5 mm might be as high as 13 m/s (g=9.8 m/s^2, μ_w=10^{-3} kg/(m·s), ρ_w-$p_g \approx 10^3$ kg/m^3).

2.2.2.2 Capillary trapping

Except for that occurring in large space like fractures, the free buoyant movement is not supposed to last long, since the upward movement of methane bubbles is accompanied by the expansion of their volumes with the decrease of the surrounding pressure (Mahabadi et al., 2018). When growing to sizes greater than throats, these methane bubbles would be trapped in the pores (i.e., capillary trapping or residual trapping). Normally, the buoyancy exerted on methane bubbles is much smaller than the auxiliary capillary resistance against these bubbles that intend to pass through throats. Accordingly, the maximum height of gas column H (L) that overlying sediments can withstand could be calculated by means of Hunt et al. (1988),

$$P_g - P_w = \frac{2\gamma cos\theta}{r} = (\rho_w - \rho_g)H \tag{7}$$

where P_g and P_w are the gas and water pressure ($ML^{-1}T^{-2}$), respectively; γ is the gas-water interfacial tension (MT^{-2}); θ is the contact angle (1); r is the radius of the narrowest throat (L). The third term of the equation represents the buoyancy exerted on the gas column with a height of H. The capillary resistance is inversely proportional to the radius of throats containing gas-water interfaces. The equation can be used to evaluate the sealing capacity of sediments for free gas, e.g., mud with a pore radius of 100 nm can withstand roughly an interconnected gas column of kilometers high (Max, 2003). Those isolated bubbles are supposedly stabilized in the pores, which holds promise for conducting the storage of greenhouse gases in aquifers (Krevor et al., 2015). In GHSZ, hydrate shells can form at the surface of these methane bubbles (Jin et al., 2012; Chen et al., 2017; Lei et al., 2019) and might hinder the upward movement of methane bubbles, since hydrate shells with certain mechanical strength could prevent the deformation of these bubbles that intend to pass through throats, as shown in Figure 2.

However, recent studies indicated that those isolated bubbles trapped in pores are only stable hydrodynamically not thermodynamically. Xu et al. (2019) suggested that gravity induces a vertical chemical potential gradient that could lead to the upward diffusion between two static bubbles, even with the same pressure. Yet, the diffusion is slow and might be negligible unless in a timescale of thousands of years.

2.2.2.3 Pressure-driven flow

When gas supply from depth is abundant, gas accumulates gradually up to its critical height that could penetrate the overlying sediments. The capillary resistance exceeds far the viscous force as gas flow is expected to be very slow, so the most favorable path is the one that connects the largest throats in

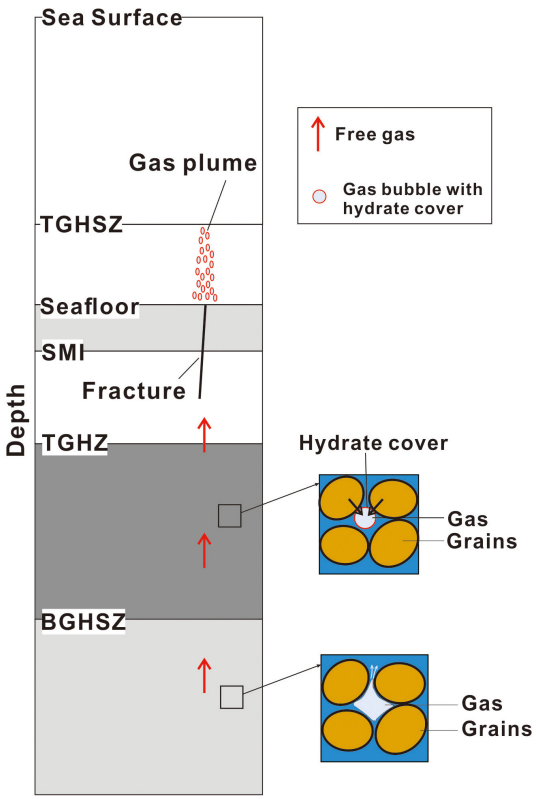

FIGURE 2
Schematics of capillary invasion of free gas bubbles and resistance from hydrate cover to capillary invasion in gas hydrate stability zone [modified from Fauria and Rempel (2011)]. Thicknesses of each layer are not to scale.

sediments (Max, 2003). At the macroscale, the gas flux q_{gas} (LT^{-1}) could be calculated by Darcy's Law in multiphase flow scenarios,

$$q_{gas} = [-\frac{kk_{rg}}{\mu_g}(\frac{\partial P_g}{\partial z} + \rho_g g)] \quad (8)$$

where k_{rg} is the relative permeability of gas phase ranging from 0 ~ 1; μ_g is the gas viscosity ($ML^{-1}T^{-1}$). The pressure gradient can be induced by the density difference between gas and water phase. Etiope (2015) suggested that the continuous gas flow can easily reach the velocities of 10^{-4} to 10^{0} cm/s (observed gas velocities) in less than 0.02 mm wide fractures, faster than the buoyant bubble movement at the same condition. However, in real marine sediments with complex structure, the continuous gas flow is limited by the relative permeability of gas phase k_{rg}.

The relative permeability k_{rg}, often expressed as the function of gas saturation S_g, could be affected by the wettability of grains, pore structures, the ratio of gas viscosity to water viscosity, the capillary curve, the measurement methods, and hydrate saturation S_h for hydrate-bearing sediments (Lijith et al., 2019). The results of Johnson et al. (2011) and Dai et al. (2019) indicated that k_{rg} in hydrate-bearing sediments is lower than the water relative permeability k_{rw} in a large range of S_g, since gas is the non-wetting phase at most time in marine sediments.

Some classical relative permeability models (usually the function of water saturation S_w) for unsaturated soils are used for marine sediments, as shown in Table 2. Jang and Santamarina (2014) suggested Corey's and van Genuchten's models are applicable in hydrate-bearing sediments by numerical simulation. Several correlations have been invoked to describe the effects of gas hydrate on empirical parameters (e.g., n_w, n_g, S_{rw}) in these relative permeability models based on numerical simulation, as shown in Table 2, suggesting lower relative permeability would be obtained at higher hydrate saturation.

2.2.2.4 Contribution of free gas flow

The free gas flow is expected to be of minor importance for methane discharge to the ocean, since isolated methane bubbles would be trapped by the capillary force and consumed gradually by hydrate formation in GHSZ, and continuous free gas flow would be limited by low relative permeability for gas phase.

TABLE 2 Relative permeability models applied in marine sediments and corresponding correlations for fitting parameters.

Model	Formula	$\bar{S}$	Fitting parameters	Reference	Correlations for fitting parameters
Van Genuchten	$k_{rw} = \bar{S}^{0.5}[1-(1-\bar{S}^{1/m})^m]^2$	$\bar{S} = (S_w - S_{rw})/(S_{wmax} - S_{rw})$	S_{rw} S_{wmax} m	(Van Genuchten, 1980)	$\begin{cases} m = m_0(1-0.19S_h) \\ S_{rw} = 0.1 + 0.17S_h \\ S_{wmax} = 1 - 0.7S_h \end{cases}$ (Mahabadi et al., 2016)
Modified Stone	$k_{rw}=[(S_w-S_{rw})/(1-S_{rw})]^{n_w}$		S_{rw} n_w n_g	(Stone, 1970)	$\begin{cases} n_w = 2.4 \ \text{avg.} \\ n_g = S_h^{0.38}/1.35 \end{cases}$ (Mahabadi and Jang, 2014)
	$k_{rg}=[(S_g-S_{rg})/(1-S_{rw})]^{n_g}$				$\begin{cases} n_w = 3.0 \sim 3.5 \\ n_g = 2 + 2.6S_h \\ S_{rw} = 0.1 + 0.17S_h \end{cases}$ (Mahabadi et al., 2016)
Corey	$k_{rw} = \bar{S}^4$ $k_{rg} = (1-\bar{S})^2(1-\bar{S}^2)$	$\bar{S} = (S_w - S_{rw})/(1 - S_{rg} - S_{rw})$		(Corey, 1954)	

However, if high-permeability conduits are present in marine sediments, the capillary force can drive gas (non-wetting phase) from marine sediments to these conduits, because the capillary force is minor in open space (Bethke et al., 1991). When these methane bubbles pass through GHSZ, hydrate shells might form at water-gas interfaces (Warzinski et al., 2014). Yet, there is limited knowledge about the competition between the fast movement of gas bubbles and hydrate formation. The effects of SD-AOM on methane bubbles are limited, since microbes can only access dissolved methane (James et al., 2016; De La Fuente et al., 2022). However, Regnier et al. (2011) suggested that if pore water reaches methane-undersaturated under the influence of the methane consumption of SD-AOM, part of the free methane gas could re-dissolve and contribute to the flux of dissolved methane accessible to microbes. These methane bubbles could migrate along high-permeability conduits with a high velocity, potentially move across seafloor, and form gas plumes in the water column (Römer et al., 2019). Seabed features linked to gas release, such as pockmarks, mud volcanoes, and cold seeps, reflect gas migration along sub-seabed high-permeability conduits (Sultan et al., 2020). The free gas movement along high-permeability conduits is seen as a dominant methane transport mechanism (Saunders et al., 1999). For example, Torres et al. (2002) observed methane bubbles escaping from subsurface conduits at a velocity of ~1 m/s on Hydrate Ridge.

2.2.3 Sediment failures

Although overpressure is a critical driving force for the upward migration of water or gas phase, the increase of fluid pressure P_f (gas or water pressure) might lead to sediment failures due to the decrease of effective stress σ' (= σ - P_f, assuming Biot's coefficient a =1). Once sediments fail, these failures provide new pathways for methane escape and could be classified into fracture initiation, fault slips, and large-scale submarine landslides according to scale.

Hydrate-bearing sediments can generally resist the occurrence of sediment failures due to the enhancement of gas hydrate on sediment strength. The enhancement from gas hydrate has been widely observed in multiple types of sediments including coarse-grained (Ebinuma et al., 2005; Masui et al., 2005; Yun et al., 2007) or fine-grained sediments (Yun et al., 2007), in laboratory tests (Winters et al., 2007; Yun et al., 2007; Miyazaki et al., 2011), and in *in-situ* measurements (Yun et al., 2006; Sultan et al., 2007), as listed in Table 3. Generally, gas hydrate exists in the form of cementation by interconnecting grains or pore occupation by bearing load, and thus enhances geomechanical strength of sediments (Waite et al., 2009; Lijith et al., 2019; Wu et al., 2020). The effects of gas hydrate could be described from the perspective of hydrate saturation and hydrate morphology. The strength, cohesion (C), stiffness (E), and Poisson's ratio (v) of sediments increase with hydrate saturation, while the internal friction angle Φ s generally insensitive to hydrate saturation (Waite et al., 2009; Lijith et al., 2019; Wu et al., 2020), with several corresponding empirical models listed in Table 4. With respect to the effects of hydrate morphology on the strength of marine sediments, cementing hydrate might have a more striking effect on mechanical properties than pore-filling hydrate, as suggested by previous experiments or numerical simulation (Ebinuma et al., 2005; Masui et al., 2005; Ding et al., 2022). However, the models considering the effects of hydrate morphology are currently rare and should be developed in the future.

2.2.3.1 Fracture initiation

A number of geophysical data indicated that fractures develop commonly in marine sediments (Krabbenhoeft et al., 2013; Plaza-Faverola et al., 2015; Elger et al., 2018; Ma et al., 2021). Except for those interpreted by tectonic activities,

TABLE 3 Summary of experimental or numerical tests on geomechanical properties of hydrate-bearing sediments.

Hydrate type	Sample types	Method	Key findings	Reference
CH_4	Artificial sandy sediments	Triaxial tests	• The shear strength and stiffness of sediments are increased prominently even by a small amount of gas hydrate. • The modes of hydrate occurrence have an important effect on the strength characteristics of the hydrate-saturated specimens.	(Ebinuma et al., 2005)
CH_4	Toyoura sand	Triaxial tests	• The proportional correlation between the shear strength and hydrate saturation degree is obtained.	(Masui et al., 2005)
CH_4	Natural sediments from the Mackenzie Delta; Ottawa sand; Clayey silt	Triaxial tests	• The magnitude of the increase of shear strength is related to hydrate saturation and hydrate cementation characteristics.	(Winters et al., 2007)
CH_4	Toyoura sand; silica sand	Triaxial tests	• The strength and stiffness of hydrate-bearing sediments increase with hydrate saturation and with the effective confining pressure. • The effect of hydrate saturation on Poisson's ratio is minor.	(Miyazaki et al., 2011)
CH_4	Clayey sediments	Triaxial tests	• The strength of the sediments is reduced by hydrate dissociation, and the strength tended to decrease further at the lower confining pressures. • The decrease in strength was mainly affected by the reduction of cohesive force.	(Song et al., 2014)
CO_2	Sand; Silt	Direct shear	• Stress state and hydrate saturation are dominant factors controlling both the stiffness and the strength of hydrate-bearing sediments. • Hydrate contributes mainly the cohesion of hydrate-bearing sediments. The cohesion increases with hydrate saturation. • The internal friction angle has no clear dependence on hydrate saturation.	(Liu et al., 2018)
		Discrete element method (DEM); Biaxial tests	• The shear strength and secant modulus (stiffness) of hydrate-bearing sediments increase with hydrate saturation regardless of the hydrate morphology. • The shear strength is slightly but the secant modulus (stiffness) is significantly influenced by hydrate morphology. The cementing type of hydrate-bearing sediments exhibits the largest secant modulus.	(Ding et al., 2022)
Tetrahydrofuran	Sand; Crushed silt; Precipitated silt; Kaolinite	Triaxial tests	• The stress-strain behavior of hydrate-bearing sediments is dependent of particle size, confining pressure, and hydrate saturation. • The peak strength of the samples increases nonlinearly with hydrate saturation. • Hydrate-bearing sediments exhibit high stiffness at low strains.	(Yun et al., 2007)

most fractures might be associated with overpressure (Daigle and Dugan, 2010; Elger et al., 2018). It should be noted that when gas and liquid phase coexists in marine sediments, gas is always the phase initiating fractures, since the gas phase has higher pressure than the water phase in water-wetting marine sediments (Daigle et al., 2020). If the internal pressure of gas bubbles exceeds their surrounding stress, these bubbles would expand by displacing neighboring grains, with new pathways generated. In a passive margin (i.e., the vertical maximum principal stress σ_1 and the horizontal minimum principal stress σ_3), these secondary fractures would open horizontally and propagate vertically (Daigle et al., 2020), and even evolve

TABLE 4 Several correlations of geomechanical properties and S_h.

Geomechanical parameters	Definition	Empirical correlations with S_h	Reference	Description
C	The component of shear strength of sediments.	$C=a+b(S_h)^2$	(Song et al., 2014; Liu et al., 2018; Lijith et al., 2019)	The cohesion C of hydrate-bearing sediments increases with S_h.
$\boldsymbol{\Phi}$	Reflecting the internal friction between grains during shearing.		(Waite et al., 2009; Song et al., 2014; Liu et al., 2018; Lijith et al., 2019)	The internal friction angle $\boldsymbol{\Phi}$ has no clear dependence on S_h.
E	The extent to which sediments resists deformation.	$E/\sigma_3' = a + bS_h^{2.5}$	(Yun et al., 2007; Miyazaki et al., 2011; Song et al., 2014; Liu et al., 2018; Lijith et al., 2019; Ding et al., 2022)	The stiffness E of hydrate-bearing sediments increases significantly with S_h.
v	The ratio between lateral strain and axial strain	0.1~0.3	(Miyazaki et al., 2011)	The effects of S_h on Poisson's ratio are not noticeable.

Note that Lijith et al. (2019) obtained the empirical correlations listed above only by fitting current available data. More experiments need to be conducted to confirm these correlations.

into pipe structures if overpressure is high enough (Elger et al., 2018; Chen et al., 2021).

Previous studies suggested that there exists a critical size V_r (L^3) for gas bubbles in marine sediments by likening marine sediments to linear elastic media (Boudreau et al., 2005; Barry et al., 2010; Algar et al., 2011b; Algar et al., 2011b; Algar et al., 2011a). When reaching their critical sizes, gas bubbles would move upward continuously with the crack propagating vertically. The $V_r(L^3)$ could be calculated as follows (Algar et al., 2011a),

$$V_r = \frac{16(1-\nu^2)\rho_s g a_r^4}{3E} \tag{9}$$

where ν is Poisson's ratio (1); E is Young's modulus ($ML^{-1}T^{-2}$); ρ_s is the bulk density of sediments (ML^{-3}); a_r is the critical half-length of crack (L), which could be calculated as follows (Algar et al., 2011a),

$$a_r = \left(\frac{3K_{IC}\sqrt{\pi}}{10\rho_s g}\right)^{2/3} \tag{10}$$

where K_{IC} is the tensile fracture toughness ($ML^{-1/2}T^{-2}$), inversely proportional to porosity of marine sediments reported by Johnson et al. (2012). Algar et al. (2011a) suggested that the spontaneous rise velocities of gas bubbles in soft sediments are on the order of centimeters per second based on numerical simulation.

Yet, at the macroscale, the mathematical models considering such spontaneous rise of gas bubbles are rare currently. Some researchers employed a simpler tensile failure criterion to consider the fracturing process (Scandella et al., 2011; Jin et al., 2015; Stranne et al., 2017; Liu et al., 2019; Daigle et al., 2020), as shown in Figure 3,

$$P_f > \sigma_3 + Tor - T > \sigma' \tag{11}$$

where P_f is the fluid pressure ($ML^{-1}T^{-2}$); σ_3 is the minimum principal stress ($ML^{-1}T^{-2}$), normally horizontal stress in passive margin (Dugan and Sheahan, 2012; Daigle et al., 2020) ($ML^{-1}T^{-2}$); T is the tensile strength ($ML^{-1}T^{-2}$); $\sigma'(=\sigma - P_f)$ is the effective stress ($ML^{-1}T^{-2}$).

The results obtained based on the assumption of tensile failure reproduce the episodic fashion of gas release in nature (Scandella et al., 2011; Stranne et al., 2017). In fact, the occurrence of fracture initiation is related to not only the magnitude of overpressure, but burial depth and stress state (Fauria and Rempel, 2011), clay content (Terzariol et al., 2021), and hydrate saturation. It should be noted that fine-grained sediments cannot guarantee their seal capacity for free gas, since free gas would crack the sediments before reaching the entry pressure, considering that the entry pressure might be higher than its geomechanical strength in fine-grained sediments.

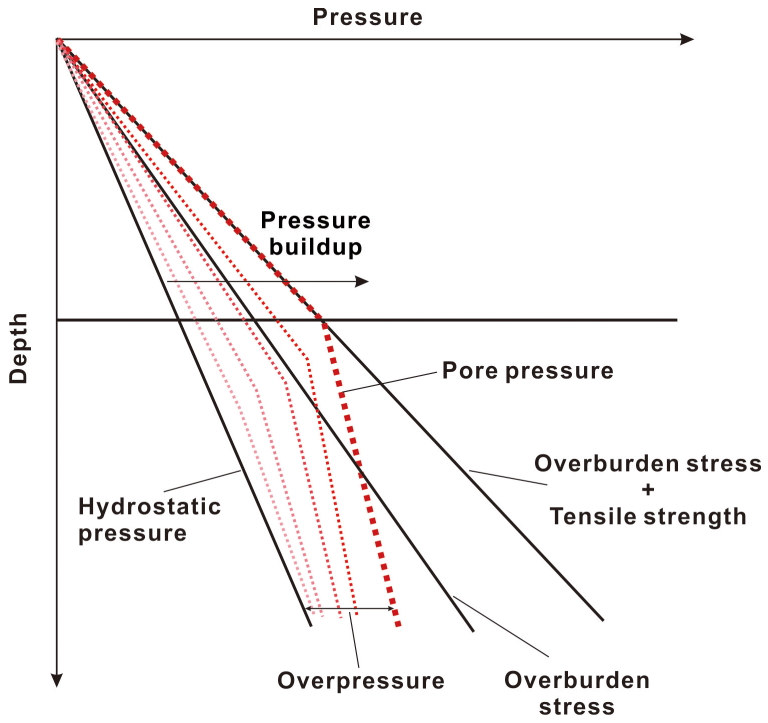

FIGURE 3
Illustration of pressure buildup in marine sediments [modified from Scandella et al. (2011)]. Sediments would be fractured if pore pressure reaches critical stress.

2.2.3.2 Fault slips

Fault slips, essentially shear failures, refer to the phenomena that the hanging wall and foot wall slip along fault planes. Fault slips could therefore be predicted by Mohr-Coulomb (MC) criterion, as shown in Figure 4,

$$\tau_f = C + \sigma_n' tan \quad \Phi \tag{12}$$

where τ_f is the shear stress at failure ($ML^{-1}T^{-2}$); C is the cohesion force ($ML^{-1}T^{-2}$), which is near zero for weak-cementing or non-cementing faults; σ'_n is the normal effective stress ($ML^{-1}T^{-2}$); Φ is the friction angle.

Fault slips could be caused by some abrupt activities such as earthquakes (Ostanin et al., 2013), or slow pressure buildup of gas phase (Hornbach et al., 2004). Hornbach et al. (2004) proposed a model to calculate the critical gas pressure that could trigger fault slips,

$$P_f = \frac{(\sigma_h + \sigma_v)/2 + [(\sigma_h - \sigma_v)/2](cos2\theta - sin2\theta/\mu) + C/\mu}{a} \tag{13}$$

where σ_h and σ_v are the total horizontal stress and vertical stress ($ML^{-1}T^{-2}$), respectively; θ is the fault/fracture angle; μ is the coefficient of sliding friction; a is Biot's coefficient.

2.2.3.3 Submarine landslides

Submarine landslides, essentially shear failures of marine sediments, refer to the downward and outward movement of slope-forming materials along one or several surfaces (Hampton et al., 1996). On a slope scale, landslides are one kind of large-scale seafloor destabilization (Talling et al., 2014). Landslides are

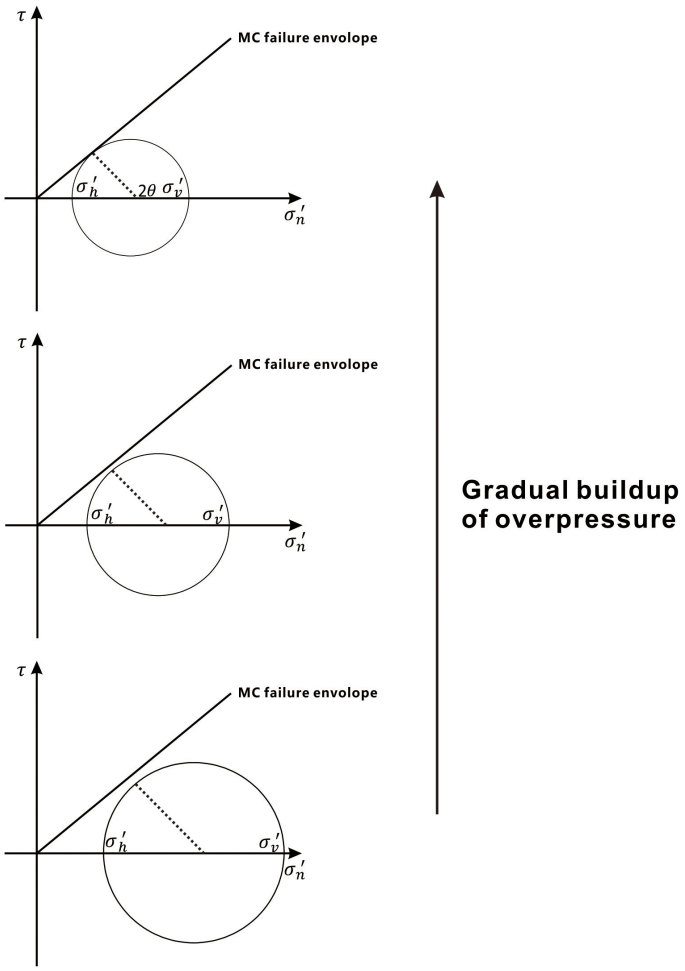

FIGURE 4
Illustration of the occurrence of fault slips, given the fault cohesion is near zero. The process of the gradual buildup of overpressure represent certain scenarios, such as slow gas accumulation beneath hydrate-bearing layers. The increase of overpressure lowers the effective stress and moves the Mohr's circle to the left [modified from Hornbach et al. (2004)]. σ'_n is the effective normal stress; σ'_v and σ'_h are the effective vertical stress and the effective horizontal stress, respectively; τ is the shear stress; θ is the fault angle.

violent ways for methane release, the amount of which is regulated by the amount of free gas beneath sliding surfaces. The safety factor *FS* was proposed to predict potential submarine landslides of slopes,

$$FS = \frac{[(\sigma_v - \rho_f gz)cos^2\theta - u^*] + C}{(\sigma_v - \rho_f gz)cos\theta sin\theta} tan\phi_f \quad (14)$$

where θ is the seafloor angle; ϕ_f is the internal angle of friction; u^* is overpressure (P_f - $\rho_f gz$, $ML^{-1}T^{-2}$). The equation provides a relation between the magnitude of overpressure and the potential of slope failures (landslides occur when $FS < 1$). Silver and Dugan (2020) employed the equation to investigate the influence of clay content on submarine slope failure through laboratory experiment and numerical simulation.

Landslides could be caused by the weight increase of overlying water, rapid sedimentation, fluid flow, cyclic wave loading, and earthquakes (Hampton et al., 1996). On continental margins, the dissociation of gas hydrate could also potentially trigger submarine landslides, since hydrate dissociation lowers the geomechanical strength of marine sediments and the released gas reduces the effective stress of marine sediments (e.g., the Storegga slides offshore of Norway reported in Paull et al. (1991) and the Cape Fear slides on the South Carolina continental rise reported in Paull et al. (1996)), as illustrated by Figure 5.

2.2.3.4 Contribution of sediment failures

The methane discharge alongside these sediment failures is expected to be great, since methane escape accompanied by abrupt pressure release is violent in short time. For example, fault slips have been invoked to explain large-scale methane release in paleo-ocean (Hornbach et al., 2004). The methane discharge associated with sediment failures is supposedly episodic most time (Stranne et al., 2017), since pressure buildup is much slower than pressure release. These dynamic processes should be considered in future work for constraining the methane flux to the ocean.

2.2.4 Gas flow through hydrate channels

Based on the phenomena that hydrate covers would form rapidly at the surface of methane bubbles in GHSZ, a new mechanism for methane migration was proposed recently. When gas supply is continuously abundant, hydrate films forming at water-gas interfaces construct tube-like hydrate channels for gas flow (Fu et al., 2020; Meyer et al., 2020), which is termed as the crustal fingering (Fu et al., 2020). Mass transfer across hydrate films is dependent on the diffusion through the films, since hydrate channels separate methane gas from water physically. Given that the diffusion coefficient of methane through hydrate films is as low as 10^{-14} to 10^{-17} m^2/s (Davies et al., 2010), the hydrate channels could construct new pathways for gas flow. These tube-like hydrate channels have been observed in experiments (Katsuki et al., 2007; Jin et al., 2012), numerical simulation (Fu et al., 2018; Fu et al., 2020), and field surveys (Fu et al., 2021). Meyer et al. (2018) proposed a schematic hydrate formation model associated with hydrate channels to explain the reason why the measured hydrate saturation was much lower than that predicted, as shown in Figure 6. Meyer et al. (2020) derived a corresponding mathematical formula of hydrate growth rate R_{CH4} ($nL^{-3}T^{-1}$),

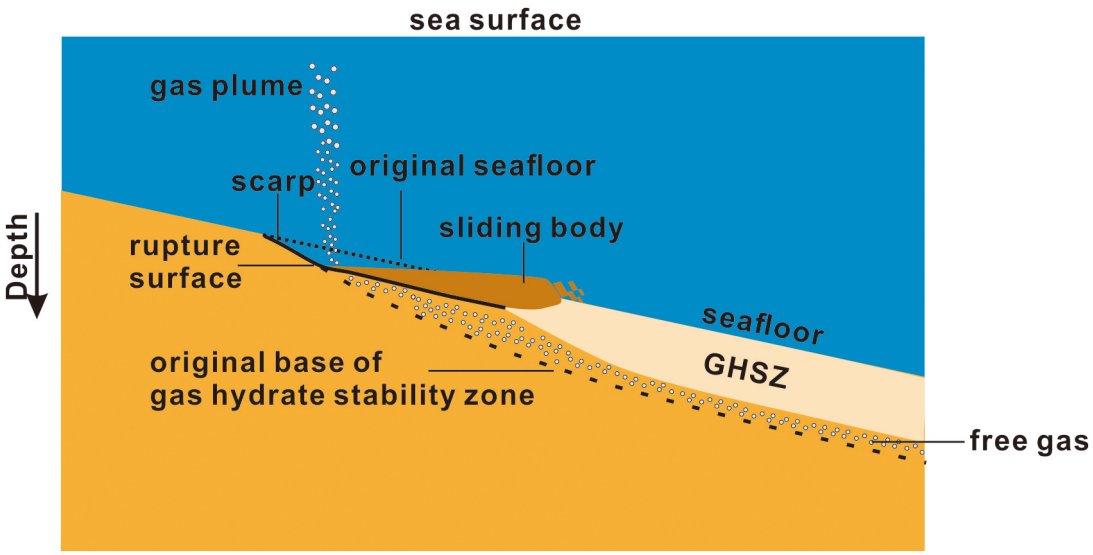

FIGURE 5
Schematic of submarine landslide caused by gas hydrate dissociation [modified from Dickens (2003)].

$$R_{CH4} = \frac{9(1-\varphi)^2 s_g^2}{\varphi S_H r_{grain}^2 M_m} D_m (C_{mg} - C_{mw}) \quad (15)$$

Where φ is the porosity (1); r_{grain} is the median grain radius (L); M_m is the molecular weight of methane (Mn^{-1}); D_m is the diffusion coefficient of methane through hydrate films (L^2T^{-1}); C_{mg} and C_{mw} are the methane concentrations in methane hydrate in contact with free gas and water (ML^{-3}), respectively.

The recently-recognized mechanism challenges the concept of the seal capacity of hydrate-bearing sediments, since the hydrate channels could protect gas from being consumed and facilitate upward methane migration.

2.2.4.1 Contribution of gas flow through hydrate channels

The hydrate formation rate obtained from the hydrate channel growth model is much slower than that predicted by traditional kinetic equations of hydrate formation proposed by Kim et al. (1987), so this new hydrate formation model could partly explain how methane gas moves through GHSZ. Although the hydrate channels have been observed at seafloor (Fu et al., 2021), more experiments are required to confirm the occurrence of long-distance hydrate channels in the course of methane gas migration through porous sediments. It is still little understood at which condition the channel-assisted gas movement would dominate methane migration, although Fu et al. (2020) suggested that the rate and frequency of gas supply determine whether vertical hydrate channels could occur.

To our current knowledge, we infer that this mechanism might be dominant in the case that gas supply from depth is abundant and continuous. If the long-distance hydrate channels can be constructed, free methane gas might migrate from depth to seafloor. However, it is still hard to constrain how much methane could escape to the ocean through hydrate channels. If the channel-assisted gas movement is proved a widespread mechanism, the effects of hydrate channels need to be incorporated into the macroscopic simulation in future work, which could help constrain the methane flux to the ocean more accurately.

3 Discussion

These mechanisms for methane migration shown in Figure 7 might occur at the same time or in succession. For example, O'hara et al. (1995) suggested water flow could also be driven by the movement of gas bubbles. Fauria and Rempel (2011) observed a transition of the migration mechanism of free gas from capillary invasion at bottom sediments to sediment fracturing at top sediments even within a single invasion episode.

Previous researchers proposed several migration mechanisms to explain the methane source of hydrate formation, e.g., local methane diffusion (Malinverno, 2010), short-range advective migration (Nole et al., 2016), and long-range fluid advection and free gas flow (Wei et al., 2022).

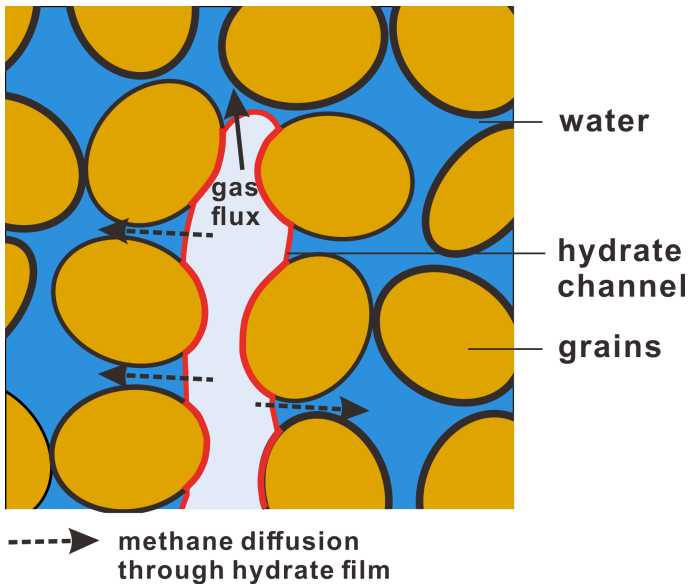

FIGURE 6
Schematic of gas flow through a hydrate channel [modified from Meyer et al. (2020)].

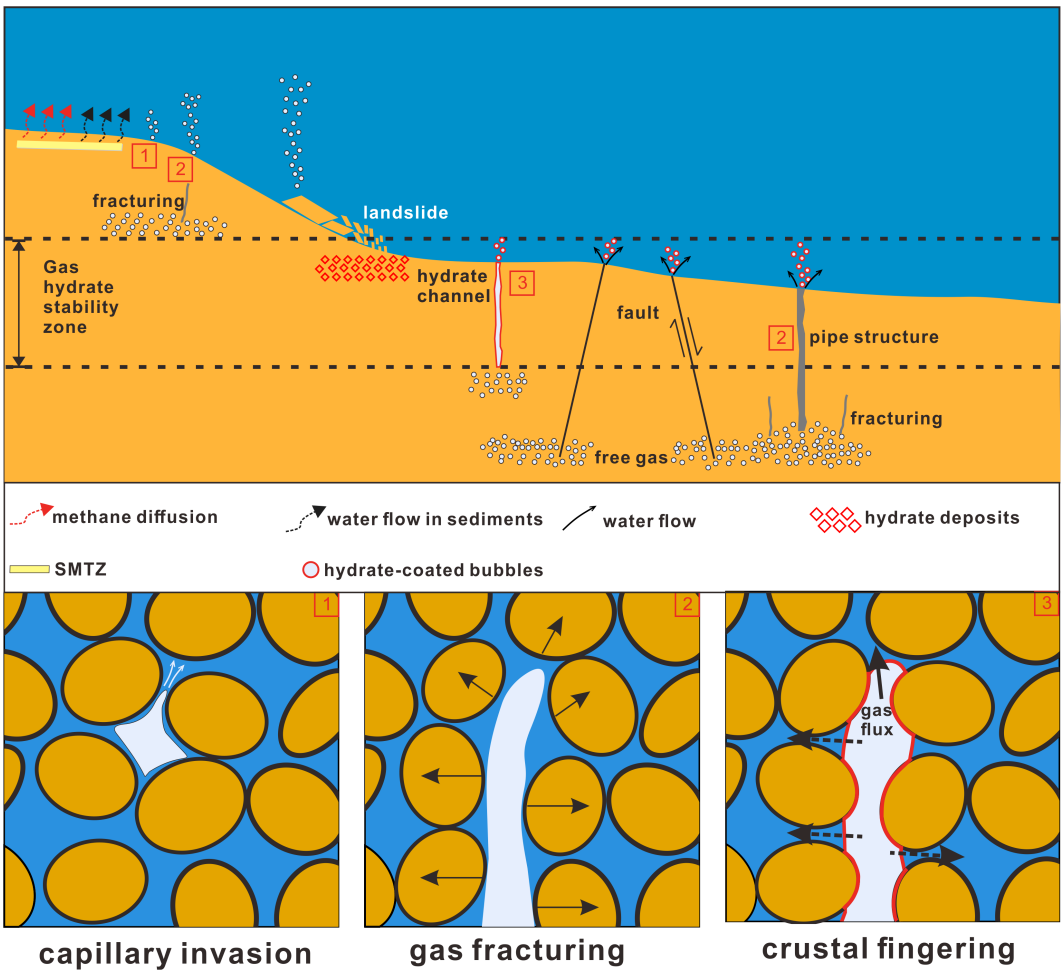

FIGURE 7
A comprehensive illustration of various mechanisms for methane migration [modified from Ma et al. (2021)].

Considering these mechanisms associated with hydrate formation, our study unifies gas hydrate systems, methane migration, and methane seepage. Compared with previous study (James et al., 2016), this study incorporates some mechanisms not mentioned before, such as sediment failures and gas flow through hydrate channels. Here, we provide a comprehensive understanding of different methane migration mechanisms associated with gas hydrate systems that can cause methane seepage.

In gas hydrate systems, in addition to the methane consumption caused by hydrate formation, the presence of gas hydrate could affect methane migration in three ways,

- preventing upward methane migration through water/gas flow by reducing the permeability of marine sediments;
- preventing upward methane migration through sediment failures by enhancing the geomechanical strength of marine sediments;
- benefiting upward methane migration by constructing hydrate channels at the interface of continuous gas columns.

Among these effects, there is an obvious contradiction. The effect of gas hydrate depends on hydrate morphology, methane phase state, and sediment type. The first effect generally occurs in coarse-grained sediments in which gas hydrate occupies pore space without completely blocking flow space for water or methane gas. The second effect commonly occurs in less permeable sediments, typically fine-grained sediments or sediments with hydrate clog where the flow resistance of fluid is higher than critical failure stress. The third effect reflects the

dynamic process of hydrate growth, requiring the involvement of methane gas.

4 Conclusions and outlook

As discussed above, methane generated in marine sediments might move upward to the ocean by certain mechanisms. These mechanisms for methane transport could be classified into diffusion and advection which includes water movement, free gas flow, sediment failures, and gas flow through hydrate channels.

- Diffusion is one of the most fundamental mechanisms for methane migration. The diffusive methane flux can be calculated by Fick's law involved with the effective methane diffusion coefficient and the dissolved methane concentration gradient. Due to the high consumption rate for methane in the gas hydrate stability zone and sulfate-methane transition zone, dissolved methane could hardly escape to the ocean by means of diffusion.
- Water movement or free gas flow are closely related to the permeability of marine sediments and the overpressure gradient of gas or liquid phase. Generally, the gas hydrate stability zone and sulfate-methane transition zone could still capture most of the dissolved methane so that few methane could reach the overlying water column by water movement. For free methane gas, marine sediments can hold isolated gas bubbles stably by the capillary force. However, the existence of high-permeability conduits might benefit water and gas migration and thus lead to a higher methane flux to the ocean.
- Sediment failures can generate new pathways for methane escape, acting as another non-negligible mechanism for methane migration. The failure modes include fracture initiation, fault slips, and submarine landslides. The methane discharge alongside sediment failure is episodic sometime, since gas/water pressure buildup is generally much slower than pressure release.
- Gas flow through hydrate channels is one recently-recognized mechanism that can partly explain how methane gas moves through the gas hydrate stability zone, challenging the concept of the seal capacity of hydrate-bearing sediments. However, more investigation is necessary to have a full understanding about the contribution of hydrate channels to the methane flux to the ocean.

As summarized in Table 5, dissolved methane from depth would be depleted in GHSZ and SMTZ and free methane would be arrested by capillary trapping. However, methane migration along preexisting fractures or sediment failure surfaces, might be considerable, since the velocity of methane movement exceeds far the rate of methane consumption (i.e., hydrate formation and methane oxidation). In addition, methane migration through hydrate channels might be ignored by previous researchers.

Although advances have been made about the methane migration mechanisms through marine sediments, further theoretical and experimental studies are necessary to have a better understanding in the following aspects,

(1) Considering that high-permeability conduits in sediments are important pathways for methane seepage, their seepage properties for gas and water flow (e.g., permeability, relative permeability, and capillary curve) are critical inputs for the estimation of the methane flux at the macroscale. However, the studies on seepage properties of these conduits are currently scarce. More experiments should be conducted to clarify the flow characteristics of high-permeability conduits quantitatively.

(2) The geomechanical properties of marine sediments are critical parameters for predicting the occurrence of sediment failures that are important ways for methane release. Although hydrate-bearing sediments exhibit

TABLE 5 Summary of mechanisms for methane transport.

Mass transfer type	Migration mechanism	Methane state	Are there new pathways generated?	Pathways	Main resistance to methane transport	Methane flux to ocean
Diffusion	Methane diffusion	Dissolved methane	N	Sediments	GHSZ and SMTZ	Low
Advection	Water movement	Dissolved methane	N	Sediments	GHSZ and SMTZ	Low
			N	Faults		High
	Free gas flow	Free methane	N	Sediments	GHSZ and Capillary trapping	Low
			N	Faults		High
	Sediment failures	Dissolved methane/ Free methane	Y	Failure surfaces		High
	Crustal fingering	Free methane	Y	Hydrate channels		Uncertain

enhanced geomechanical properties, reliable constitutive models describing the hydrate effect are still rare. More investigations should be focused on the quantitative correlations of geomechanical properties and hydrate distribution including hydrate saturation and morphology.

(3) As a recently-recognized mechanism, gas flow through hydrate channels might constitute a part of the methane flux to the ocean. However, the occurrence of hydrate channels in the course of methane transport is still little known. More experiments should be conducted to confirm the occurrence conditions of hydrate channels.

Author contributions

HLu supervised the study; HLiu wrote the original draft; LZ and HLu contributed to refining the draft. All authors contributed to the article and approved the submitted version.

Funding

This work is supported by the China Geological Survey (grant number: DD20221703).

Conflict of interest

The authors declare that the research was conducted in the absence of any commercial or financial relationships that could be construed as a potential conflict of interest.

Publisher's note

All claims expressed in this article are solely those of the authors and do not necessarily represent those of their affiliated organizations, or those of the publisher, the editors and the reviewers. Any product that may be evaluated in this article, or claim that may be made by its manufacturer, is not guaranteed or endorsed by the publisher.

References

Algar, C. K., Boudreau, B. P., and Barry, M. A. (2011a). Initial rise of bubbles in cohesive sediments by a process of viscoelastic fracture. *J. Geophys. Res.-Solid Earth* 116(B4), B04207. doi: 10.1029/2010jb008133

Algar, C. K., Boudreau, B. P., and Barry, M. A. (2011b). Release of multiple bubbles from cohesive sediments. *Geophys. Res. Lett.* 38(8), L08606. doi: 10.1029/2011gl046870

Atkins, P., and de Paula, J. (2021) *Physical chemistry for the life science*. Available at: https://chem.libretexts.org/@go/page/1392 (Accessed March 7 2022).

Barnes, R., and Goldberg, E. (1976). Methane production and consumption in anoxic marine sediments. *Geology* 4 (5), 297–300. doi: 10.1130/0091-7613(1976)4<297:MPACIA>2.0.CO;2

Barry, M., Boudreau, B., Johnson, B., and Reed, A. (2010). First-order description of the mechanical fracture behavior of fine-grained surficial marine sediments during gas bubble growth. *J. Geophys. Res.: Earth Surf.* 115 (F4), F04029. doi: 10.1029/2010JF001833

Bear, J. (1988). *Dynamics of fluids in porous media* (North Chelmsford: Courier Corporation).

Berndt, C. (2005). Focused fluid flow in passive continental margins. *Philos. Trans. R. Soc. A: Math. Phys. Eng. Sci.* 363 (1837), 2855–2871. doi: 10.1098/rsta.2005.1666

Bethke, C. M. (1986). Inverse hydrologic analysis of the distribution and origin of gulf coast-type geopressured zones. *J. Geophys. Res.: Solid Earth* 91 (B6), 6535–6545. doi: 10.1029/JB091iB06p06535

Bethke, C. M., Reed, J. D., and Oltz, D. F. (1991). Long-range petroleum migration in the Illinois basin. *AAPG Bull.* 75 (5), 925–945. doi: 10.1306/0C9B2899-1710-11D7-8645000102C1865D

Boswell, R., and Collett, T. S. (2011). Current perspectives on gas hydrate resources. *Energy Environ. Sci.* 4 (4), 1206–1215. doi: 10.1039/c0ee00203h

Boudreau, B. P., Algar, C., Johnson, B. D., Croudace, I., Reed, A., Furukawa, Y., et al. (2005). Bubble growth and rise in soft sediments. *Geology* 33 (6), 517–520. doi: 10.1130/G21259.1

Brereton, G. J., Crilly, R. J., and Spears, J. R. (1998). Nucleation in small capillary tubes. *Chem. Phys.* 230 (2-3), 253–265. doi: 10.1016/S0301-0104(98)00052-4

Cao, C., Cai, F., Qi, H. S., Zhao, S. H., and Wu, C. Q. (2021). Differences in the sulfate-methane transitional zone in coastal pockmarks in various sedimentary environments. *Water* 13 (1), 68. doi: 10.3390/w13010068

Cardoso, S. S., and Cartwright, J. H. (2016). Increased methane emissions from deep osmotic and buoyant convection beneath submarine seeps as climate warms. *Nat. Commun.* 7, 13266. doi: 10.1038/ncomms13266

Chen, L.-T., Li, N., Sun, C.-Y., Chen, G.-J., Koh, C. A., and Sun, B.-J. (2017). Hydrate formation in sediments from free gas using a one-dimensional visual simulator. *Fuel* 197, 298–309. doi: 10.1016/j.fuel.2017.02.034

Chen, D., Zhang, G., Dong, D., Zhao, M., and Wang, X. (2021). Widespread fluid seepage related to buried submarine landslide deposits in the northwestern south China Sea. *Geophys. Res. Lett.* 49 (6), e2021GL096584. doi: 10.1029/2021GL096584

Corey, A. T. (1954). The interrelation between gas and oil relative permeabilities. *Producers mon.* 19 (1), 38–41.

Daigle, H., Cook, A., Fang, Y., Bihani, A., Song, W., and Flemings, P. B. (2020). Gas-driven tensile fracturing in shallow marine sediments. *J. Geophys. Res.: Solid Earth* 125, e2020JB020835. doi: 10.1029/2020JB020835

Daigle, H., and Dugan, B. (2010). Origin and evolution of fracture-hosted methane hydrate deposits. *J. Geophys. Res.: Solid Earth* 115 (B11), B11103. doi: 10.1029/2010JB007492

Dai, S., Kim, J., Xu, Y., Waite, W. F., Jang, J., Yoneda, J., et al. (2019). Permeability anisotropy and relative permeability in sediments from the national gas hydrate program expedition 02, offshore India. *Mar. Petrol. Geol.* 108, 705–713. doi: 10.1016/j.marpetgeo.2018.08.016

Dai, S., and Seol, Y. (2014). Water permeability in hydrate-bearing sediments: A pore-scale study. *Geophys. Res. Lett.* 41 (12), 4176–4184. doi: 10.1002/2014GL060535

Dale, A. W., Regnier, P., Van Cappellen, P., Fossing, H., Jensen, J., and Jørgensen, B. (2009). Remote quantification of methane fluxes in gassy marine sediments through seismic survey. *Geology* 37 (3), 235–238. doi: 10.1130/G25323A.1

Dale, A. W., Van Cappellen, P., Aguilera, D. R., and Regnier, P. (2008). Methane efflux from marine sediments in passive and active margins: Estimations from bioenergetic reaction-transport simulations. *Earth Planet. Sci. Lett.* 265 (3-4), 329–344. doi: 10.1016/j.epsl.2007.09.026

Darcy, H. (1856). *Les Fontaines publiques de la ville de Dijon: exposition et application* (Paris: Victor Dalmont).

Davies, S. R., Sloan, E. D., Sum, A. K., and Koh, C. A. (2010). *In situ* studies of the mass transfer mechanism across a methane hydrate film using high-resolution confocal raman spectroscopy. *J. Phys. Chem. C* 114 (2), 1173–1180. doi: 10.1021/jp909416y

Davie, M., Zatsepina, O. Y., and Buffett, B. (2004). Methane solubility in marine hydrate environments. *Mar. geol.* 203 (1-2), 177–184. doi: 10.1016/S0025-3227(03)00331-1

De La Fuente, M., Arndt, S., Marin-Moreno, H., and Minshull, T. A. (2022). Assessing the benthic response to climate-driven methane hydrate destabilisation: State of the art and future modelling perspectives. *Energies* 15 (9), 3307. doi: 10.3390/en15093307

Delsontro, T., McGinnis, D. F., Sobek, S., Ostrovsky, I., and Wehrli, B. (2010). Extreme methane emissions from a Swiss hydropower reservoir: Contribution from bubbling sediments. *Environ. Sci. Technol.* 44 (7), 2419–2425. doi: 10.1021/es9031369

Dessandier, P. A., Knies, J., Plaza-Faverola, A., Labrousse, C., Renoult, M., and Panieri, G. (2021). Ice-sheet melt drove methane emissions in the Arctic during the last two interglacials. *Geology* 49 (7), 799–803. doi: 10.1130/G48580.1

Dickens, G. R. (2003). Rethinking the global carbon cycle with a large, dynamic and microbially mediated gas hydrate capacitor. *Earth Planet. Sci. Lett.* 213 (3-4), 169–183. doi: 10.1016/S0012-821x(03)00325-X

Ding, Y., Qian, A., Lu, H., Li, Y., and Zhang, Y. (2022). DEM investigation of the effect of hydrate morphology on the mechanical properties of hydrate-bearing sands. *Comput. Geotech.* 143, 104603. doi: 10.1016/j.compgeo.2021.104603

Duan, Z., and Weare, J. H. (1992). The prediction of methane solubility in natural-waters to high ionic-strength from 0-Degrees-C to 250-Degrees-C and from 0 bar to 1600 bar - reply. *Geochim. Et Cosmochim. Acta* 56 (12), 4303–4303. doi: 10.1016/0016-7037(92)90271-J

Dugan, B., and Flemings, P. B. (2000). Overpressure and fluid flow in the new Jersey continental slope: Implications for slope failure and cold seeps. *Science* 289 (5477), 288–291. doi: 10.1126/science.289.5477.288

Dugan, B., and Sheahan, T. (2012). Offshore sediment overpressures of passive margins: Mechanisms, measurement, and models. *Rev. Geophys.* 50 (3), RG3001. doi: 10.1029/2011RG000379

Ebinuma, T., Kamata, Y., Minagawa, H., Ohmura, R., Nagao, J., and Narita, H. (2005). "Mechanical properties of sandy sediment containing methane hydrate," In: *Fifth International Conference on Gas Hydrates*. (Trondheim, Norway: Tapir Acad).

Egger, M., Riedinger, N., Mogollon, J. M., and Jorgensen, B. B. (2018). Global diffusive fluxes of methane in marine sediments. *Nat. Geosci.* 11 (6), 421–42+. doi: 10.1038/s41561-018-0122-8

Elger, J., Berndt, C., Rüpke, L., Krastel, S., Gross, F., and Geissler, W. H. (2018). Submarine slope failures due to pipe structure formation. *Nat. Commun.* 9 (1), 1–6. doi: 10.1038/s41467-018-03176-1

Etiope, G. (2015). *Natural gas seepage*. (Cham: Springer Cham). doi: 10.1007/978-3-319-14601-0

Fauria, K. E., and Rempel, A. W. (2011). Gas invasion into water-saturated, unconsolidated porous media: Implications for gas hydrate reservoirs. *Earth Planet. Sci. Lett.* 312 (1-2), 188–193. doi: 10.1016/j.epsl.2011.09.042

Fick, A. (1855). Ueber diffusion. *Annalen der Physik* 170 (1), 59–86. doi: 10.1002/andp.18551700105

Flemings, P. B., Liu, X. L., and Winters, W. J. (2003). Critical pressure and multiphase flow in Blake ridge gas hydrates. *Geology* 31 (12), 1057–1060. doi: 10.1130/G19863.1

Fu, X. J., Cueto-Felgueroso, L., and Juanes, R. (2018). Nonequilibrium thermodynamics of hydrate growth on a gas-liquid interface. *Phys. Rev. Lett.* 120 (14), 144501. doi: 10.1103/PhysRevLett.120.144501

Fujii, T., Suzuki, K., Takayama, T., Tamaki, M., Komatsu, Y., Konno, Y., et al. (2015). Geological setting and characterization of a methane hydrate reservoir distributed at the first offshore production test site on the daini-atsumi knoll in the eastern nankai trough, Japan. *Mar. Petrol. Geol.* 66, 310–322. doi: 10.1016/j.marpetgeo.2015.02.037

Fu, X., Jimenez-Martinez, J., Nguyen, T. P., Carey, J. W., Viswanathan, H., Cueto-Felgueroso, L., et al. (2020). Crustal fingering facilitates free-gas methane migration through the hydrate stability zone. *Proc. Natl. Acad. Sci.* 117 (50), 31660. doi: 10.1073/pnas.2011064117

Fu, X., Waite, W. F., and Ruppel, C. D. (2021). Hydrate formation on marine seep bubbles and the implications for water column methane dissolution. *J. Geophys. Res.-Oceans* 126 (9), e2021JC017363. doi: 10.1029/2021JC017363

Ginsburg, G. D., and Soloviev, V. A. (1997). Methane migration within the submarine gas-hydrate stability zone under deep-water conditions. *Mar. Geol.* 137 (1-2), 49–57. doi: 10.1016/S0025-3227(96)00078-3

Graham, K., and Westbrook, (2009). Escape of methane gas from the seabed along the West spitsbergen continental margin. *Geophys. Res. Lett* 36, L15608. doi: 10.1029/2009GL039191

Haacke, R. R., Westbrook, G. K., and Hyndman, R. D. (2007). Gas hydrate, fluid flow and free gas: Formation of the bottom-simulating reflector. *Earth Planet. Sci. Lett.* 261 (3-4), 407–420. doi: 10.1016/j.epsl.2007.07.008

Hampton, M. A., Lee, H. J., and Locat, J. (1996). Submarine landslides. *Rev. geophys.* 34 (1), 33–59. doi: 10.1029/95RG03287

Handa, Y. P. (1990). Effect of hydrostatic pressure and salinity on the stability of gas hydrates. *J. Phys. Chem.* 94 (6), 2652–2657. doi: 10.1021/j100369a077

Henry, P., Thomas, M., and Ben Clennell, M. (1999). Formation of natural gas hydrates in marine sediments 2. thermodynamic calculations of stability conditions in porous sediments. *J. Geophys. Res.-Solid Earth* 104 (B10), 23005–23022. doi: 10.1029/1999jb900167

Hornbach, M. J., Bangs, N. L., and Berndt, C. (2012). Detecting hydrate and fluid flow from bottom simulating reflector depth anomalies. *Geology* 40 (3), 227–230. doi: 10.1130/g32635.1

Hornbach, M. J., Saffer, D. M., and Holbrook, W. S. (2004). Critically pressured free-gas reservoirs below gas-hydrate provinces. *Nature* 427 (6970), 142–144. doi: 10.1038/nature02172

Hou, J., Ji, Y., Zhou, K., Liu, Y., and Wei, B. (2018). Effect of hydrate on permeability in porous media: Pore-scale micro-simulation. *Int. J. Heat Mass Transf.* 126, 416–424. doi: 10.1016/j.ijheatmasstransfer.2018.05.156

Hsu, S. K., Wang, S. Y., Liao, Y. C., Yang, T. Y. F., Jan, S., Lin, J. Y., et al. (2013). Tide-modulated gas emissions and tremors off SW Taiwan. *Earth Planet. Sci. Lett.* 369, 98–107. doi: 10.1016/j.epsl.2013.03.013

Hunt, J. R., Sitar, N., and Udell, K. S. (1988). Nonaqueous phase liquid transport and cleanup: 1. analysis of mechanisms. *Water Resour. Res.* 24 (8), 1247–1258. doi: 10.1029/WR024i008p01247

Islam, M. (2004). Einstein–Smoluchowski diffusion equation: a discussion. *Physica Scripta* 70 (2-3), 120. doi: 10.1088/0031-8949/70/2-3/008

Iversen, N., and Jørgensen, B. B. (1993). Diffusion coefficients of sulfate and methane in marine sediments: Influence of porosity. *Geochim. Cosmochim. Acta* 57 (3), 571–578. doi: 10.1016/0016-7037(93)90368-7

James, R. H., Bousquet, P., Bussmann, I., Haeckel, M., Kipfer, R., Leifer, I., et al. (2016). Effects of climate change on methane emissions from seafloor sediments in the Arctic ocean: A review. *Limnol. Oceanogr.* 61 (S1), S283–S299. doi: 10.1002/lno.10307

Jang, J., and Santamarina, J. C. (2014). Evolution of gas saturation and relative permeability during gas production from hydrate-bearing sediments: Gas invasion vs. gas nucleation. *J. Geophys. Res.: Solid Earth* 119 (1), 116–126. doi: 10.1002/2013JB010480

Jin, Z. H., Johnson, S. E., and Cook, A. E. (2015). Crack extension induced by dissociation of fracture-hosted methane gas hydrate. *Geophys. Res. Lett.* 42 (20), 8522–8529. doi: 10.1002/2015GL066060

Jin, Y., Konno, Y., and Nagao, J. (2012). Growth of methane clathrate hydrates in porous media. *Energy Fuels* 26 (4), 2242–2247. doi: 10.1021/ef3001357

Johnson, B. D., Barry, M. A., Boudreau, B. P., Jumars, P. A., and Dorgan, K. M. (2012). *In situ* tensile fracture toughness of surficial cohesive marine sediments. *Geo-Marine Lett.* 32 (1), 39–48. doi: 10.1007/s00367-011-0243-1

Johnson, A., Patil, S., and Dandekar, A. J. M. (2011). Experimental investigation of gas-water relative permeability for gas-hydrate-bearing sediments from the mount Elbert gas hydrate stratigraphic test well, Alaska north slope. *Mar. Petrol. Geol.* 28 (2), 419–426. doi: 10.1016/j.marpetgeo.2009.10.013

Kang, D. H., Yun, T. S., Kim, K. Y., and Jang, J. (2016). Effect of hydrate nucleation mechanisms and capillarity on permeability reduction in granular media. *Geophys. Res. Lett.* 43 (17), 9018–9025. doi: 10.1002/2016gl070511

Katsuki, D., Ohmura, R., Ebinuma, T., and Narita, H. (2007). Methane hydrate crystal growth in a porous medium filled with methane-saturated liquid water. *Philos. Mag.* 87 (7), 1057–1069. doi: 10.1080/14786430601021652

Keller, M., and Stallard, R. F. (1994). Methane emission by bubbling from gatun lake, Panama. *J. Geophys. Res.-Atmos.* 99 (D4), 8307–8319. doi: 10.1029/92jd02170

Kim, H., Bishnoi, P. R., Heidemann, R. A., and Rizvi, S. S. (1987). Kinetics of methane hydrate decomposition. *Chem. Eng. Sci.* 42 (7), 1645–1653. doi: 10.1016/0009-2509(87)80169-0

Kleinberg, R., Flaum, C., Griffin, D., Brewer, P., Malby, G., Peltzer, E., et al. (2003). Deep sea NMR: Methane hydrate growth habit in porous media and its relationship to hydraulic permeability, deposit accumulation, and submarine slope stability. *J. Geophys. Res.: Solid Earth* 108 (B10), 2508. doi: 10.1029/2003JB002389

Konno, Y., Oyama, H., Nagao, J., Masuda, Y., and Kurihara, M. (2010). Numerical analysis of the dissociation experiment of naturally occurring gas hydrate in sediment cores obtained at the Eastern nankai trough, Japan. *Energy Fuels* 24 (12), 6353–6358. doi: 10.1021/ef1008727

Krabbenhoeft, A., Bialas, J., Klaucke, I., Crutchley, G., Papenberg, C., and Netzeband, G. L. (2013). Patterns of subsurface fluid-flow at cold seeps: The hikurangi margin, offshore new Zealand. *Mar. Petrol. Geol.* 39 (1), 59–73. doi: 10.1016/j.marpetgeo.2012.09.008

Krevor, S., Blunt, M. J., Benson, S. M., Pentland, C. H., Reynolds, C., Al-Menhali, A., et al. (2015). Capillary trapping for geologic carbon dioxide storage – from pore

scale physics to field scale implications. *Int. J. Greenhouse Gas Control* 40, 221–237. doi: 10.1016/j.ijggc.2015.04.006

Kumar, A., Maini, B., Bishnoi, P. R., Clarke, M., Zatsepina, O., and Srinivasan, S. (2010). Experimental determination of permeability in the presence of hydrates and its effect on the dissociation characteristics of gas hydrates in porous media. *J. Petrol. Sci. Eng.* 70 (1-2), 114–122. doi: 10.1016/j.petrol.2009.10.005

Lei, L., Seol, Y., and Myshakin, E. M. (2019). Methane hydrate film thickening in porous media. *Geophys. Res. Lett.* 46 (20), 11091–11099. doi: 10.1029/2019gl084450

Lijith, K. P., Malagar, B. R. C., and Singh, D. N. (2019). A comprehensive review on the geomechanical properties of gas hydrate bearing sediments. *Mar. Petrol. Geol.* 104, 270–285. doi: 10.1016/j.marpetgeo.2019.03.024

Linke, P., Suess, E., Torres, M., Martens, V., Rugh, W., Ziebis, W., et al. (1994). *In situ* measurement of fluid flow from cold seeps at active continental margins. *Deep Sea Res. Part I: Oceanogr. Res. Pap.* 41 (4), 721–739. doi: 10.1016/0967-0637(94)90051-5

Liu, Z., Dai, S., Ning, F., Peng, L., Wei, H., and Wei, C. (2018). Strength estimation for hydrate-bearing sediments from direct shear tests of hydrate-bearing sand and silt. *Geophys. Res. Lett.* 45 (2), 715–723. doi: 10.1002/2017gl076374

Liu, J. L., Haeckel, M., Rutqvist, J., Wang, S. H., and Yan, W. (2019). The mechanism of methane gas migration through the gas hydrate stability zone: Insights from numerical simulations. *J. Geophys. Res.-Solid Earth* 124 (5), 4399–4427. doi: 10.1029/2019jb017417

Li, G., Wu, D.-M., Li, X.-S., Lv, Q.-N., Li, C., and Zhang, Y. (2017). Experimental measurement and mathematical model of permeability with methane hydrate in quartz sands. *Appl. Energy* 202, 282–292. doi: 10.1016/j.apenergy.2017.05.147

Li, J. F., Ye, J. L., Qin, X. W., Qiu, H. J., Wu, N. Y., Lu, H. L., et al. (2018). The first offshore natural gas hydrate production test in south China Sea. *China Geol.* 1 (1), 5–16. doi: 10.31035/cg2018003

Li, C., Zhan, L., and Lu, H. (2022). Mechanisms for overpressure development in marine sediments. *J. Mar. Sci. Eng.* 10 (4), 490. doi: 10.3390/jmse10040490

Mahabadi, N., Dai, S., Seol, Y., Sup Yun, T., and Jang, J. (2016). The water retention curve and relative permeability for gas production from hydrate-bearing sediments: pore-network model simulation. *Geochem. Geophys. Geosyst.* 17 (8), 3099–3110. doi: 10.1002/2016gc006372

Mahabadi, N., and Jang, J. (2014). Relative water and gas permeability for gas production from hydrate-bearing sediments. *Geochem. Geophys. Geosyst.* 15 (6), 2346–2353. doi: 10.1002/2014gc005331

Mahabadi, N., Zheng, X. L., Yun, T. S., van Paassen, L., and Jang, J. (2018). Gas bubble migration and trapping in porous media: Pore-scale simulation. *J. Geophys. Res.-Solid Earth* 123 (2), 1060–1071. doi: 10.1002/2017jb015331

Malinverno, A. (2010). Marine gas hydrates in thin sand layers that soak up microbial methane. *Earth Planet. Sci. Lett.* 292 (3-4), 399–408. doi: 10.1016/j.epsl.2010.02.008

Masuda, Y., Naganawa, S., and Ando, S. (1997). "Numerical calculation of gas production performance from reservoirs containing natural gas hydrates," in *Annual technical conference* (San Antonio, Tex.: Soc. of Petrol. Eng.).

Masui, A., Haneda, H., Ogata, Y., and Aoki, K. (2005). "The effect of saturation degree of methane hydrate on the shear strength of synthetic methane hydrate sediments," In: *Fifth International Conference on Gas Hydrates*. (Trondheim, Norway: Tapir Acad).

Mau, S., Tu, T. H., Becker, M., Ferreira, C. D., Chen, J. N., Lin, L. H., et al. (2020). Methane seeps and independent methane plumes in the south China Sea offshore Taiwan. *Front. Mar. Sci.* 7. doi: 10.3389/fmars.2020.00543

Max, M. D. (2003). *Natural gas hydrate in oceanic and permafrost environments* (Berlin: Springer Science & Business Media).

Ma, G., Zhan, L., Lu, H., and Hou, G. (2021). Structures in shallow marine sediments associated with gas and fluid migration. *J. Mar. Sci. Eng.* 9 (4), 396. doi: 10.3390/jmse9040396

Mello, U. T., Karner, G. D., and Anderson, R. N. (1994). A physical explanation for the positioning of the depth to the top of overpressure in shale-dominated sequences in the gulf coast basin, united states. *J. Geophys. Res.: Solid Earth* 99 (B2), 2775–2789. doi: 10.1029/93JB02899

Meyer, D. W., Flemings, P. B., DiCarlo, D., You, K., Phillips, S. C., and Kneafsey, T. J. (2018). Experimental investigation of gas flow and hydrate formation within the hydrate stability zone. *J. Geophys. Res.: Solid Earth* 123 (7), 5350–5371. doi: 10.1029/2018jb015748

Meyer, D. W., Flemings, P. B., You, K., and DiCarlo, D. A. (2020). Gas flow by invasion percolation through the hydrate stability zone. *Geophys. Res. Lett.* 47 (3), e2019GL084380. doi: 10.1029/2019GL084380

Miller, R. D. (1980). Freezing phenomena in soils. *Appl. Soil phys.* (New York: Acad. Press), 254–299. doi: 10.1016/B978-0-12-348580-9.50016-X

Miyazaki, K., Masui, A., Sakamoto, Y., Aoki, K., Tenma, N., and Yamaguchi, T. (2011). Triaxial compressive properties of artificial methane-hydrate-bearing sediment. *J. Geophys. Res.* 116 (B6), B06102. doi: 10.1029/2010jb008049

Moridis, G. (2014). *User's manual of the TOUGH+ core code v1. 5: A general-purpose simulator of non-isothermal flow and transport through porous and fractured media*. California, United States: Lawrence Berkeley National Laboratory. doi: 10.2172/1165986

Nauhaus, K., Boetius, A., Krüger, M., and Widdel, F. (2002). *In vitro* demonstration of anaerobic oxidation of methane coupled to sulphate reduction in sediment from a marine gas hydrate area. *Environ. Microbiol.* 4 (5), 296–305. doi: 10.1046/j.1462-2920.2002.00299.x

Nole, M., Daigle, H., Cook, A. E., and Malinverno, A. (2016). Short-range, overpressure-driven methane migration in coarse-grained gas hydrate reservoirs. *Geophys. Res. Lett.* 43 (18), 9500–9508. doi: 10.1002/2016gl070096

O'hara, S., Dando, P., Schuster, U., Bennis, A., Boyle, J., Chui, F., et al. (1995). Gas seep induced interstitial water circulation: observations and environmental implications. *Continent. Shelf Res.* 15 (8), 931–948. doi: 10.1016/0278-4343(95)80003-V

Osborne, M. J., and Swarbrick, R. E. (1997). Mechanisms for generating overpressure in sedimentary basins: A reevaluation. *AAPG Bull.* 81 (6), 1023–1041. doi: 10.1306/522B49C9-1727-11D7-8645000102C1865D

Ostanin, I., Anka, Z., di Primio, R., and Bernal, A. (2013). Hydrocarbon plumbing systems above the snøhvit gas field: structural control and implications for thermogenic methane leakage in the hammerfest basin, SW barents Sea. *Mar. Petrol. Geol.* 43, 127–146. doi: 10.1016/j.marpetgeo.2013.02.012

Pan, L., Lei, L., and Seol, Y. (2021). Pore-scale influence of methane hydrate on permeability of porous media. *J. Natural Gas Sci. Eng.* 87, 103758. doi: 10.1016/j.jngse.2020.103758

Paull, C. K., Buelow, W. J., Ussler, W.III, and Borowski, W. S. (1996). Increased continental-margin slumping frequency during sea-level lowstands above gas hydrate–bearing sediments. *Geology* 24 (2), 143–146. doi: 10.1130/0091-7613(1996)024<0143:ICMSFD>2.3.CO;2

Paull, C. K., Ussler, W.III, and Dillon, W. P. (1991). Is the extent of glaciation limited by marine gas-hydrates? *Geophys. Res. Lett.* 18 (3), 432–434. doi: 10.1029/91GL00351

Perkins, T., and Johnston, O. (1963). A review of diffusion and dispersion in porous media. *Soc. Petrol. Eng. J.* 3 (01), 70–84. doi: 10.2118/480-PA

Plaza-Faverola, A., Bünz, S., Johnson, J. E., Chand, S., Knies, J., Mienert, J., et al. (2015). Role of tectonic stress in seepage evolution along the gas hydrate-charged vestnesa ridge, fram strait. *Geophys. Res. Lett.* 42 (3), 733–742. doi: 10.1002/2014gl062474

Reagan, M. T., Moridis, G. J., Elliott, S. M., and Maltrud, M. (2011). Contribution of oceanic gas hydrate dissociation to the formation of Arctic ocean methane plumes. *J. Geophys. Res.: Oceans* 116 (C9), C09014. doi: 10.1029/2011JC007189

Reeburgh, W. S. (2007). Oceanic methane biogeochemistry. *Chem. Rev.* 107 (2), 486–513. doi: 10.1021/cr050362v

Regnier, P., Dale, A. W., Arndt, S., LaRowe, D. E., Mogollon, J., and Van Cappellen, P. (2011). Quantitative analysis of anaerobic oxidation of methane (AOM) in marine sediments: A modeling perspective. *Earth-Sci. Rev.* 106 (1-2), 105–130. doi: 10.1016/j.earscirev.2011.01.002

Ren, X. W., Guo, Z. Y., Ning, F. L., and Ma, S. Z. (2020). Permeability of hydrate-bearing sediments. *Earth-Sci. Rev.* 202, 103100. doi: 10.1016/j.earscirev.2020.103100

Römer, M., Hsu, C.-W., Loher, M., MacDonald, I. R., dos Santos Ferreira, C., Pape, T., et al. (2019). Amount and fate of gas and oil discharged at 3400 m water depth from a natural seep site in the southern gulf of Mexico. *Front. Mar. Sci.* 6. doi: 10.3389/fmars.2019.00700

Ruppel, C. D., and Kessler, J. D. (2017). The interaction of climate change and methane hydrates. *Rev. Geophys.* 55 (1), 126–168. doi: 10.1002/2016rg000534

Ruppel, C. D., and Waite, W. F. (2020). Timescales and processes of methane hydrate formation and breakdown, with application to geologic systems. *J. Geophys. Res.: Solid Earth* 125 (8), e2018JB016459. doi: 10.1029/2018JB016459

Saunders, D. F., Burson, K. R., and Thompson, C. K. (1999). Model for hydrocarbon microseepage and related near-surface alterations. *AAPG Bull.* 83 (1), 170–185. doi: 10.1306/00AA9A34-1730-11D7-8645000102C1865D

Sauter, E. J., Muyakshin, S. I., Charlou, J. L., Schluter, M., Boetius, A., Jerosch, K., et al. (2006). Methane discharge from a deep-sea submarine mud volcano into the upper water column by gas hydrate-coated methane bubbles. *Earth Planet. Sci. Lett.* 243 (3-4), 354–365. doi: 10.1016/j.epsl.2006.01.041

Scandella, B. P., Varadharajan, C., Hemond, H. F., Ruppel, C., and Juanes, R. (2011). A conduit dilation model of methane venting from lake sediments. *Geophys. Res. Lett.* 38 (6), L06408. doi: 10.1029/2011GL046768

Shen, P., Li, G., Li, B., and Li, X. (2020). Coupling effect of porosity and hydrate saturation on the permeability of methane hydrate-bearing sediments. *Fuel* 269, 117425. doi: 10.1016/j.fuel.2020.117425

Silver, M. M. W., and Dugan, B. (2020). The influence of clay content on submarine slope failure: insights from laboratory experiments and numerical models. *Geol. Soc. London Special. Publ.* 500 (1), 301–309. doi: 10.1144/sp500-2019-186

Song, Y., Zhu, Y., Liu, W., Zhao, J., Li, Y., Chen, Y., et al. (2014). Experimental research on the mechanical properties of methane hydrate-bearing sediments during hydrate dissociation. *Mar. Petrol. Geol.* 51, 70–78. doi: 10.1016/j.marpetgeo.2013.11.017

Spinelli, G. A., Giambalvo, E. R., and Fisher, A. T. (2004). "Sediment permeability, distribution, and influence on fluxes in oceanic basement," In *Hydrogeology of the Oceanic Lithosphere with CD-ROM* (Cambridge: Cambridge University Press).

Stocker, T. (2014). Climate change 2013: the physical science basis: Working Group I contribution to the Fifth assessment report of the Intergovernmental Panel on Climate Change. (Cambridge: Cambridge University Press)

Stone, H. (1970). Probability model for estimating three-phase relative permeability. *J. petrol. Technol.* 22 (02), 214–218. doi: 10.2118/2116-PA

Stranne, C., O'Regan, M., and Jakobsson, M. (2017). Modeling fracture propagation and seafloor gas release during seafloor warming-induced hydrate dissociation. *Geophys. Res. Lett.* 44 (16), 8510–8519. doi: 10.1002/2017GL074349

Stranne, C., O'Regan, M., Jakobsson, M., Brüchert, V., and Ketzer, M. (2019). Can anaerobic oxidation of methane prevent seafloor gas escape in a warming climate? *Solid Earth* 10 (5), 1541–1554. doi: 10.5194/se-10-1541-2019

Sultan, N., Plaza-Faverola, A., Vadakkepuliyambatta, S., Buenz, S., and Knies, J. (2020). Impact of tides and sea-level on deep-sea Arctic methane emissions. *Nat. Commun.* 11 (1), 1–10. doi: 10.1038/s41467-020-18899-3

Sultan, N., Voisset, M., Marsset, T., Vernant, A. M., Cauquil, E., Colliat, J. L., et al. (2007). Detection of free gas and gas hydrate based on 3D seismic data and cone penetration testing: An example from the Nigerian continental slope. *Mar. Geol.* 240 (1-4), 235–255. doi: 10.1016/j.margeo.2007.02.012

Sun, J., Dong, H., Arif, M., Yu, L., Zhang, Y., Golsanami, N., et al. (2021). Influence of pore structural properties on gas hydrate saturation and permeability: A coupled pore-scale modelling and X-ray computed tomography method. *J. Natural Gas Sci. Eng.* 88, 103805. doi: 10.1016/j.jngse.2021.103805

Talling, P. J., Clare, M., Urlaub, M., Pope, E., Hunt, J. E., and Watt, S. F. L. (2014). Large Submarine landslides on continental slopes geohazards, methane release, and climate change. *Oceanography* 27 (2), 32–45. doi: 10.5670/oceanog.2014.38

Terzariol, M., Sultan, N., Apprioual, R., and Garziglia, S. (2021). Pore habit of gas in gassy sediments. *J. Geophys. Res.-Solid Earth* 126 (5), e2020JB021511. doi: 10.1029/2020JB021511

Timmis, K. N., McGenity, T., van der Meer, J. R., and de Lorenzo, V. (2010). *Handbook of hydrocarbon and lipid microbiology* (Berlin: Springer).

Torres, M. E., McManus, J., Hammond, D., De Angelis, M., Heeschen, K., Colbert, S., et al. (2002). Fluid and chemical fluxes in and out of sediments hosting methane hydrate deposits on hydrate ridge, OR, I: Hydrological provinces. *Earth Planet. Sci. Lett.* 201 (3-4), 525–540. doi: 10.1016/S0012-821X(02)00733-1

Tryon, M. D., Brown, K. M., Torres, M. E., Tréhu, A. M., McManus, J., and Collier, R. W. (1999). Measurements of transience and downward fluid flow near episodic methane gas vents, hydrate ridge, cascadia. *Geology* 27 (12), 1075–1078. doi: 10.1130/0091-7613(1999)027<1075:MOTADF>2.3.CO;2

Ullman, W. J., and Aller, R. C. (1982). Diffusion-coefficients in nearshore marine-sediments. *Limnol. Oceanogr.* 27 (3), 552–556. doi: 10.4319/lo.1982.27.3.0552

Van Genuchten, M. T. (1980). A closed-form equation for predicting the hydraulic conductivity of unsaturated soils. *Soil Sci. Soc. America J.* 44 (5), 892–898. doi: 10.2136/sssaj1980.03615995004400050002x

Waite, W. F., Santamarina, J. C., Cortes, D. D., Dugan, B., Espinoza, D. N., Germaine, J., et al. (2009). Physical properties of hydrate-bearing sediments. *Rev. Geophys.* 47, RG4003. doi: 10.1029/2008rg000279

Warzinski, R. P., Lynn, R., Haljasmaa, I., Leifer, I., Shaffer, F., Anderson, B. J., et al. (2014). Dynamic morphology of gas hydrate on a methane bubble in water: Observations and new insights for hydrate film models. *Geophys. Res. Lett.* 41 (19), 6841–6847. doi: 10.1002/2014GL061665

Weber, T., Wiseman, N. A., and Kock, A. (2019). Global ocean methane emissions dominated by shallow coastal waters. *Nat. Commun.* 10, 4584. doi: 10.1038/s41467-019-12541-7

Wei, L., Cook, A., and You, K. (2022). Methane migration mechanisms for the green canyon block 955 gas hydrate reservoir, northern gulf of Mexico. *AAPG Bull.* 106 (5), 1005–1023. doi: 10.1306/06022120134

Winters, W. J., Waite, W. F., Mason, D. H., Gilbert, L. Y., and Pecher, I. A. (2007). Methane gas hydrate effect on sediment acoustic and strength properties. *J. Petrol. Sci. Eng.* 56 (1-3), 127–135. doi: 10.1016/j.petrol.2006.02.003

Wu, P., Li, Y., Sun, X., Liu, W., and Song, Y. (2020). Mechanical characteristics of hydrate-bearing sediment: A review. *Energy Fuels* 35 (2), 1041–1057. doi: 10.1021/acs.energyfuels.0c03995

Xu, W., and Germanovich, L. N. (2006). Excess pore pressure resulting from methane hydrate dissociation in marine sediments: A theoretical approach. *J. Geophys. Res.: Solid Earth* 111 (B1), B01104. doi: 10.1029/2004JB003600

Xu, K., Mehmani, Y., Shang, L., and Xiong, Q. (2019). Gravity-induced bubble ripening in porous media and its impact on capillary trapping stability. *Geophys. Res. Lett.* 46 (23), 13804–13813. doi: 10.1029/2019GL085175

Xu, W. Y., and Ruppel, C. (1999). Predicting the occurrence, distribution, and evolution of methane gas hydrate in porous marine sediments. *J. Geophys. Res.-Solid Earth* 104 (B3), 5081–5095. doi: 10.1029/1998jb900092

Ye, J.-L., Qin, X.-W., Xie, W.-W., Lu, H.-L., Ma, B.-J., Qiu, H.-J., et al. (2020). The second natural gas hydrate production test in the south China Sea. *China Geol.* 3 (2), 197–209. doi: 10.31035/cg2020043

You, K., and Flemings, P. B. (2021). Methane hydrate formation and evolution during sedimentation. *J. Geophys. Res.-Solid Earth* 126 (4), e2020JB021235. doi: 10.1029/2020JB021235

You, K., Flemings, P. B., Malinverno, A., Collett, T., and Darnell, K. (2019). Mechanisms of methane hydrate formation in geological systems. *Rev. Geophys.* 57 (4), 1146–1196. doi: 10.1029/2018RG000638

Yun, T. S., Narsilio, G. A., and Carlos Santamarina, J. (2006). Physical characterization of core samples recovered from gulf of Mexico. *Mar. Petrol. Geol.* 23 (9-10), 893–900. doi: 10.1016/j.marpetgeo.2006.08.002

Yun, T. S., Santamarina, J. C., and Ruppel, C. (2007). Mechanical properties of sand, silt, and clay containing tetrahydrofuran hydrate. *J. Geophys. Res.: Solid Earth* 112 (B4), B04106. doi: 10.1029/2006jb004484

Zhang, L., Ge, K., Wang, J., Zhao, J., and Song, Y. (2020). Pore-scale investigation of permeability evolution during hydrate formation using a pore network model based on X-ray CT. *Mar. Petrol. Geol.* 113, 104157. doi: 10.1016/j.marpetgeo.2019.104157

Zhang, Y., and Zhai, W.-D. (2015). Shallow-ocean methane leakage and degassing to the atmosphere: triggered by offshore oil-gas and methane hydrate explorations. *Front. Mar. Sci.* 2. doi: 10.3389/fmars.2015.00034

Zheng, L., and Yapa, P. D. (2000). Buoyant velocity of spherical and nonspherical bubbles/droplets. *J. Hydraul. Eng.* 126 (11), 852–854. doi: 10.1061/(ASCE)0733-9429(2000)126:11(852)